https://doi.org/10.5194/ar-2025-37
Preprint. Discussion started: 12 November 2025

AEROSOL Research Discussions

Real-Time Water-Soluble Iron Speciation in Ambient Aerosols at Neutral and Slightly Acidic pH

Sabine Lüchtrath[1], Sven Klemer[1], Florian Fröhlich[1], Darius Ceburnis[2], Dominik van Pinxteren[3], Hartmut Herrmann[3], Wolfgang Frenzel[1], Andreas Held[1]

[1] Chair of Environmental Chemistry and Air Research, Technische Universität Berlin, Berlin, 10623, Germany
[2] The Ryan Institute's Centre for Climate & Air Pollution Studies (C-CAPS), University of Galway, Galway, H91 CF50, Republic of Ireland
[3] Leibniz Institute for Tropospheric Research (TROPOS), Atmospheric Chemistry Department (ACD), 04318 Leipzig, Germany.

Correspondence to: sabine.luechtrath@tu-berlin.de

Abstract. We present the first online instrument for the speciation of water-soluble iron in ambient aerosols, enabling simultaneous quantification of Fe(II) (ws-Fe(II)) and total water-soluble Fe (total ws-Fe). The system combines flow injection analysis with spectrophotometric detection of the Fe(II)–ferrozine complex using a liquid waveguide capillary cell (LWCC) for sensitive detection. The setup was tested with two different aerosol sampling units during field campaigns in Berlin. In summer 2024, the Metrohm AeRosol Sampler (MARS) operated at pH 6.5, while in winter 2025 a particle-into-liquid sampler (PILS) was applied at pH 4.5 to mimic acidic cloud water conditions. Limits of quantification (LOQ) for Fe(II) determination were 1.6 ng m^{-3} and 1.0 ng m^{-3} for the MARS-FIA and PILS-FIA setups, respectively, with ambient ws-Fe concentrations ranging from below LOQ to 47 ng m^{-3}. Both setups yielded robust online measurements; however, the PILS-FIA working at pH 4.5 underestimated ws-Fe compared to filter sampling and extraction. This discrepancy can be attributed to the shorter extraction time in the PILS system, highlighting the influence of extraction duration on the measured iron concentration. Since soluble iron drives important tropospheric aqueous-phase reactions like hydroxyl radical formation through Fenton chemistry, the speciation data provided by the presented setup could improve model representations of atmospheric iron processes.

1 Introduction

Atmospheric soluble iron concentration is of great interest for atmospheric processes, public health and ocean biochemistry. In the global biogeochemical iron cycle, atmospheric iron supports marine productivity, particularly in open ocean regions where it is suggested to regulate and even limit phytoplankton growth (Browning and Moore, 2023; Moore et al., 2013). The bioavailable fraction of atmospheric iron is assumed to be soluble (Raiswell et al., 2008; Fan et al., 2006) and can influence the ocean-atmosphere carbon cycling which in turn affects Earth's climate (Hutchins and Tagliabue, 2024; Shao et al., 2011; Jickells et al., 2005).

Furthermore, airborne soluble iron is present in either Fe(II) or Fe(III) and can thus participate in multiple atmospheric processes altering the chemical composition of aerosols (Al-Abadleh, 2024; Pehkonen et al., 1993). For example, previous studies have shown that soluble iron impacts on the formation of secondary organic aerosol (Lüchtrath et al., 2024; Chu et al.,

https://doi.org/10.5194/ar-2025-37
Preprint. Discussion started: 12 November 2025

AEROSOL Research Discussions

2017) and depending on the oxidation state, light conditions and presence of hydrogen peroxide (H_2O_2) can lead to the formation of light absorbing particles by reacting with phenolic precursors (Lüchtrath et al., 2025; De Haan et al., 2024; S. Hopstock et al., 2023; Slikboer et al., 2015) thus having a direct impact on the Earth's radiative budget.

In the aqueous phase, iron acts as a major catalyst for hydroxyl (OH) radical formation through Fenton (Fe(II) + H_2O_2) and photo-Fenton (Fe(III) + light + H_2O_2) reactions and thus enhancing the oxidation capacity of aerosol particles in atmospheric droplets (Tilgner and Herrmann, 2018; Herrmann et al., 2015; Arakaki and Faust, 1998; Zepp et al., 1992; Fenton, 1894).

On a global scale, mineral dust is the primary source of atmospheric iron; Ito and Shi, (2016) estimated that it contributes about 98 % of the total atmospheric iron budget. Freshly emitted dust exhibits very low iron solubility (Longo et al., 2016; Mahowald et al., 2009; Luo et al., 2005). During atmospheric transport, Fe-bearing minerals can dissolve through three main pathways, which are proton-promoted, ligand promoted and reductive dissolution (Al-Abadleh et al., 2024; Chen and Grassian, 2013; Rubasinghege et al., 2010). These three mechanisms are influenced by various factors like pH, particle size, presence of solar radiation, crystallinity of the Fe-bearing mineral and the Fe-organic complexes (Liu et al., 2022; Meskhidze et al., 2017; Paris and Desboeufs, 2013; Journet et al., 2008). Over the past four decades, research consistently demonstrates that iron dissolution rates are highest under acidic conditions (pH < 4), particularly when exposed to solar radiation and oxalate with nanometer-sized, amorphous iron, especially from combustion sources (Baldo et al., 2022; Ito et al., 2019).

Under typical environmental conditions, Fe(II) starts to hydrolyse at pH > 8, whereas Fe(III) hydrolysis begins already at pH > 3 (Langmuir, 1997). Atmospheric aerosols, cloud and fog droplets exhibit acidity spanning approximately 5 pH units (Pye et al., 2020). Typical pH values for cloud droplets range from 3 to 6 (Pye et al., 2020). However, most cloud droplets do not precipitate as rain; instead, they evaporate, leaving a residual thin water film around dust particles. The wet aerosols can have aqueous-phase pH values below 2 (Pye et al., 2020). Shi et al. (2015) simulated the cycling of Fe-containing particles between wet aerosols (pH 1–2) and cloud droplets (pH 5–6). They found that acidic wet aerosol conditions promote rapid dissolution of low soluble Fe-containing particles, whereas at higher pH in cloud droplets precipitation of Fe-rich nanoparticles is favored, which can rapidly re-dissolve upon droplet evaporation. The authors further emphasized that the duration of the acidic aerosol stage increases the amount of soluble iron.

As illustrated in Figure 1, combustion processes like biomass burning, industrial production but also traffic contribute only few percent to the total amount of atmospheric iron (Ito and Shi, 2016; Luo et al., 2008), but possibly make up 40–100 % of the total soluble Fe fraction (Ito, 2015; Sholkovitz et al., 2009; Luo et al., 2008). The concentrations of dissolved iron in fog and cloud water can therefore vary locally depending on environmental conditions and iron emission source, ranging between 0.002 and 647 $\mu molL^{-1}$ (Bianco et al., 2020; Deguillaume et al., 2005).

In atmospheric science literature, solubility is often defined as the percentage of dissolved Fe, measured in the filtrate after passing through a 0.2–0.45 µm pore size filter, relative to the total Fe content in the bulk aerosol sample (Shi et al., 2012). Because the concentration of Fe in the filtrate (and thus its measured solubility) depends on pH, we use the term "water soluble (ws) Fe" in this study. This includes Fe measured both in neutral water (Seradest, pH 6.5) and under slightly acidic conditions (pH 4.5), which simulate cloud water environments.

https://doi.org/10.5194/ar-2025-37
Preprint. Discussion started: 12 November 2025

A common method to determine water-soluble Fe(II) (ws-Fe(II)) in ambient aerosols (Kuang et al., 2020; Oakes et al., 2010; Rastogi et al., 2009) spectrophotometrically is the reaction between Fe(II) and ferrozine leading to the formation of a stable magenta-coloured complex developed by Stookey (1970). The reduction of Fe(III) to Fe(II) by a reductant like hydroxyl ammonium hydrochloride (HA) enables the determination of total ws-Fe and has been extensively used (Lei et al., 2023; Majestic et al., 2006; Stookey, 1970). The applied reduction time varies from some minutes (Lei et al., 2023; Kuang et al., 2020) to several hours (Yang et al., 2021).

The principle of flow injection analysis (FIA) firstly introduced by Nagy et al. (1970) is the precise introduction of sample volumes into a continuous, bubble-free stream, enabling automated analyses that are fast, accurate, and widely applicable. FIA setups have been used to determine ws-Fe(II) and total ws-Fe of different origins as natural water, waste water, potato leaves or human hair (e.g. Pullin and Cabaniss, 2001; Pascual-Reguera et al., 1997).

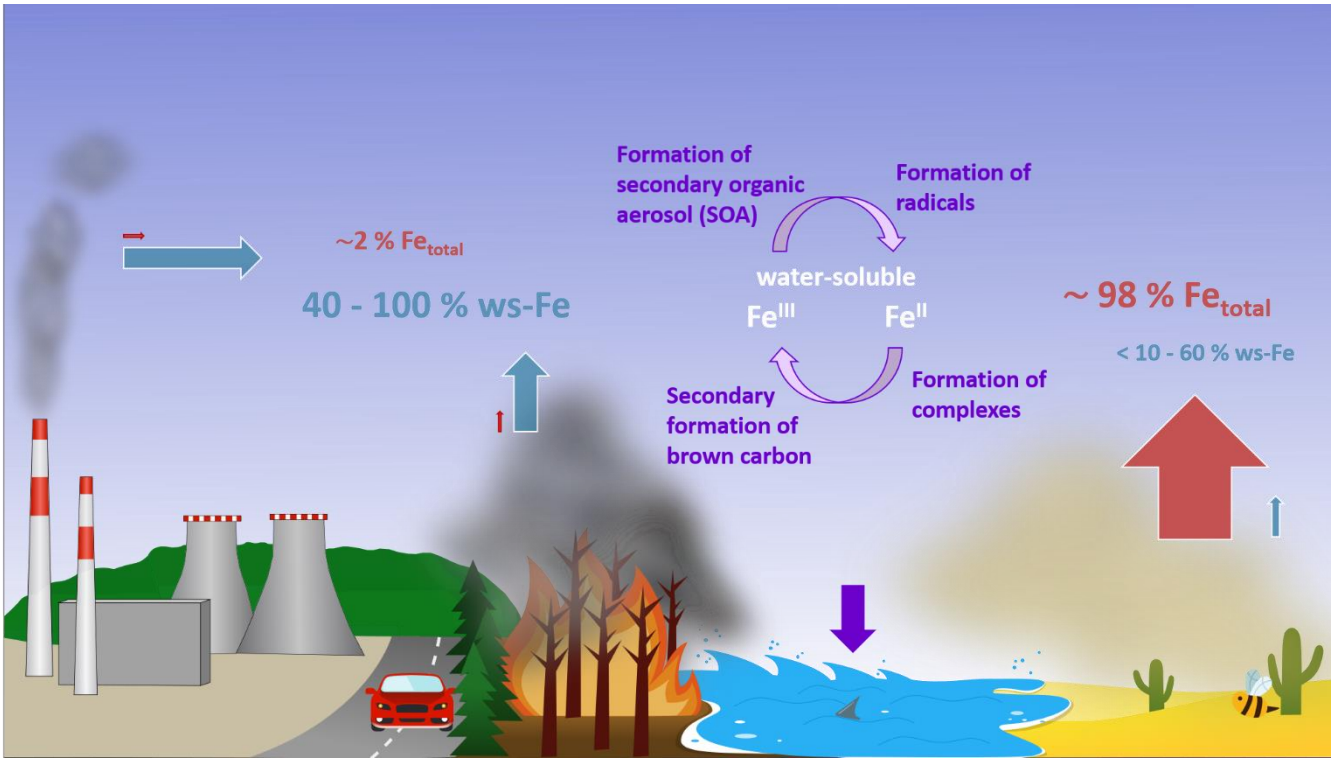

Figure 1: Sources, sinks and processes of atmospheric water-soluble iron

Aerosols are typically collected on filter for 12-24 h and analysed offline afterwards. The offline analysis limits the investigation of time resolved variability in concentrations and speciation of ws-Fe. Furthermore, the redox state of iron can change during collection and filter storage. Rastogi et al. (2009) developed the first online technique for determining water-soluble Fe(II) in ambient aerosols using a particle-into-liquid sampler coupled with a continuous flow ferrozine method.

https://doi.org/10.5194/ar-2025-37
Preprint. Discussion started: 12 November 2025

Building on the work of Rastogi et al. (2009), we present an online method combining FIA and particle-into-liquid sampling to quantify ws-Fe(II), total ws-Fe, and thereby ws-Fe(III), advancing insights into ws-Fe sources, processes of Fe dissolution and the role of iron chemistry in atmospheric processes (Figure 1).

2 Methods

2.1 Chemicals and Solution Preparation

Except for the glass volumetric flasks, only plastic bottles and beakers were used to avoid iron cross contamination. All vessels were cleaned by soaking in 0.03 M HNO_3 and rinsed with Seradest water (Seradest S750, Veolia Water Technoloies, Germany). The 0.03 M HNO_3 was prepared from bidistilled water and HNO_3 (65 %, Suprapur, Merck, Germany). A 0.8 mM HNO_3 solution was prepared to achieve a pH of 3–3.5, while a 0.04 mM HNO_3 solution was used to obtain a pH of 4.5. All working standards and solvents for the FIA system were freshly prepared daily. The iron working standards (0.5-50 $\mu g L^{-1}$) were prepared by dilution of a 1 $g L^{-1}$ Fe(II) stock solution (acidified to pH1 by HCl) of $FeSO_4 \cdot 7H_2O$ (≥99% p.a., Carl Roth GmbH, Germany) and a 1 $g L^{-1}$ Fe(III) stock solution (acidified to pH1 by HCl) of $(NH_4)_2Fe(SO_4)_2 \cdot 6H_2O$ (≥ 98%, Carl Roth GmbH, Germany). Ferrozine solutions were prepared by dissolving 133 mg Ferrozine, 3-(2-pyridyl)-5,6-diphenyl-1,2,4-triazine-4‘,4‘ ‘-disulfonic acid sodium salt (Iron reagent, hydrate, 95+%, pure, Thermo Scientific Chemicals, Germany) in 100 mL Seradest water, resulting in a 2.7 mM solution. As a reduction reagent, 19.3 mg hydroxylamine hydrochloride (99.9 %, Thermo Scientific Chemicals, Germany) was dissolved in 50 mL Seradest water. For cleaning the FIA system and the liquid waveguide capillary cell (LWCC), methanol, 2 M HCl and 2 % Hellmanex (Hellma Analytics GmbH & Co. KG, Germany) were used.

2.2 Online analysis system

A measurement setup consisting of a commercially available particle-into-liquid sampling unit and a custom-built flow injection analysis (FIA) system with a liquid waveguide capillary cell (LWCC) was developed to detect, in quasi-online mode, the concentration and oxidation state of atmospheric soluble iron. Two commercially available sampling units were used: the Metrohm AeRosol Sampler (MARS; Metrohm Process Analytics, Filderstadt, Germany) and the Particle-Into-Liquid Sampler PILS BMI 4002 (Brechtel Manufacturing Inc., USA). Concentrations of ws-Fe(II) and total ws-Fe were quantified spectrophotometrically by the ferrozine method. Ferrozine and Fe(II) form a complex with a characteristic absorbance maximum at λ = 562 nm (Stookey, 1970). Total ws-Fe was determined after reduction of Fe(III) to Fe(II) using hydroxylamine hydrochloride (HA) as reduction reagent. A scheme of the setup is shown in Figure 2. All dimensions and flow parameters are listed in Table 1. The system components will be explained in more detail in the following sections.

https://doi.org/10.5194/ar-2025-37
Preprint. Discussion started: 12 November 2025

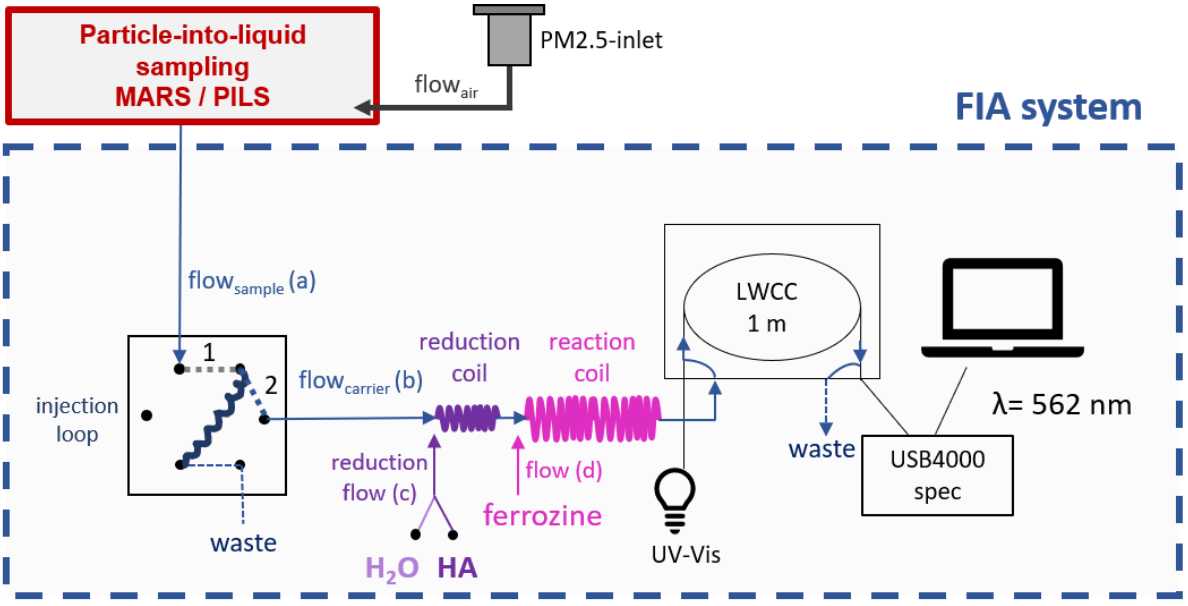

Figure 2: Schematic diagram of the measurement setup in detail

2.2.1 Particle-into-liquid sampling units

Particle-into liquid sampling units are designed to enable an online analysis of ambient aerosol bulk composition. The basic principle is based on particle growth into droplets through supersaturation of water vapor which are then collected in liquid solution (e.g. Stieger et al., 2018; Weber et al., 2001). The Metrohm AeRosol Sampler (MARS) is part of the commercial Monitor for AeRosols and Gases in ambient Air (MARGA, Metrohm, Applikon, Netherlands). Both, MARGA and PILS measurements were conducted in several studies (e.g. Zeng et al., 2021; Stieger et al., 2019) and are thus validated approaches for the online determination of water-soluble aerosol compounds.

Metrohm AeRosol Sampler (MARS)

The MARS sampler was connected to a PM2.5 inlet. The airflow of 1 $m^3\ h^{-1}$ is regulated by the usage of a critical orifice. The air flow passes the Wet Rotator Denuder (WRD) which removes soluble gases from the air stream. Aerosols will not be absorbed but follow the air stream due to their inertia. After having passed the WRD the air stream enters the Steam Jet Aerosol Collector (SJAC) where supersaturated steam is introduced by a steamer. In the steamer chamber, the particles grow by deliquescence. Due to their inertia the grown particles are separated by the cyclone and collected into the 1.2 mL sampling volume on the bottom of the SJAC. The liquid sampled is continuously transferred through a 0.45µm syringe filter to the injection loop of the FIA system. The sample flow to the FIA system was adjusted to 0.1 $mLmin^{-1}$. The sample concentration

https://doi.org/10.5194/ar-2025-37
Preprint. Discussion started: 12 November 2025

AEROSOL Research Discussions

factor (SCF) describes the ratio between the concentration in the atmosphere (c_{air}) and the liquid sample (c_{sample}) (Eq.1). The MARS-FIA system had an SCF of 6. As no internal standard was used no dilution factor was applied.

$$c_{air}\ [ng\ m^{-3}] = c_{sample}\ [\mu g\ L^{-1}] \cdot SCF \quad \text{Eq.1}$$

Particle Into Liquid Sampler (PILS)

The PILS BMI4002 is a modification of the PILS instrument described by Weber et al. (2001). Its setup and operation mode were described in detailed by Sorooshian et al. (2006). The PILS was used in online mode and operated at an air flow rate of 14.6 $Lmin^{-1}$ with a 2.5 µm diameter-cut cyclone at the inlet. No denuders were installed. In the condensation chamber, the ambient air mixes with steam leading to supersaturation and therefore particle activation. The activated particles grow to >1 µm diameter before they reach the impaction plate (Sorooshian et al., 2006). A wash flow of 0.065 mL min^{-1} transports the impacted droplets down the impactor plate from where they are transferred to the FIA system at s sample flow rate ($Flow_{Sample}$ (a)) of 0.05 $mLmin^{-1}$. The pH of an average droplet can be expected to be 5.6 (Ma, 2004; Sorooshian et al., 2006). To test whether Fe-solubility is increased by lowering the pH of the sample, the wash flow was slightly acidified to pH 4.5 using 0.04 mM HNO_3. During particle collection, liquid from the droplets and the transport flow solution can dilute the sample. Additionally, water condenses on the impaction plate. Orsini et al. (2003) quantified this additional water as 5 to 20 µL min^{-1}. As no internal standard was used in this study and the wash flow was 1.3 times higher than the sample flow, a dilution factor of 1.5 was applied, assuming an average additional condensed water contribution of 10 µL min^{-1}. The SCF for the PILS system was 5.13.

Blank measurements of both sampling units were conducted regularly by directing the airflow through a HEPA zero filter (HEPA-CAP, Whatman, UK). The filter was connected for one hour prior to measurement. Blank values were then determined from the subsequent two hours of sampling. The limit of quantification (LOQ) was defined as ten times and the limit of detection (LOD) three times the standard deviation of the blank values (Eq.2 &3) and were determined for ws-Fe(II) and total ws-Fe.

$$LOD = 3 \cdot \sigma_{blanks} \quad \text{Eq. 2}$$

$$LOQ = 10 \cdot \sigma_{blanks} \quad \text{Eq. 3}$$

https://doi.org/10.5194/ar-2025-37
Preprint. Discussion started: 12 November 2025

Table 1: Overview of dimensions and operational parameters for MARS - and PILS-FIA systems

	MARS	PILS
Cut off diameter	2.5 µm	2.5 µm
$Flow_{air}$	16.7 L min^{-1}	14.6 L min^{-1}
SCF	6	5.13
Injection volume	600 µL	400 µL
$Flow_{sample}$ (a)	0.1 mL min^{-1}	0.05 mL min^{-1}
Sampling time	10 min	12 min
pH of sampling flow	5.5 – 6.0	4.5
FIA $flow_{carrier}$ (b)	1.0 mL min^{-1}	0.5 mL min^{-1}
FIA ferrozine flow (c)	0.1 mL min^{-1}	0.05 mL min^{-1}
FIA reduction flow (d)	0.1 mL min^{-1}	0.05 mL min^{-1}
reaction coil	800 cm	800 cm
reaction time	78 s	157 s
reduction coil	200 cm	200 cm
reduction time	20 s	40 s
Total tubing length	1080 cm	1080 cm
Tubing diameter	0.5 mm	0.5 mm
LWCC volume	250 µL	250 µL
$LOD_{Fe,\ total}$	0.48 n gm^{-3}	0.15 ng m^{-3}
$LOD_{Fe(II)}$	0.39 n gm^{-3}	0.3 ng m^{-3}
$LOQ_{Fe,total}$	1.6 n gm^{-3}	0.5 ng m^{-3}
$LOQ_{Fe(II)}$	1.3 n gm^{-3}	1.0 ng m^{-3}
$Blank_{Fe\ total}$	1.84± 0.16 n gm^{-3}	3.51±0.10 n gm^{-3}
$Blank_{Fe2+}$	1.01± 0.12 n gm^{-3}	0.84± 0.05 ng m^{-3}

2.2.2 Flow Injection Analysis Unit

A three-line flow injection analysis system was developed to quantify soluble iron in liquid samples using spectrophotometric detection. Ferrous iron (Fe(II)) forms a stable magenta complex with ferrozine which absorbs at 562 nm, enabling its detection. This method was originally introduced by Stookey (1970). A previous reduction of present Fe(III) further enables the determination of the total soluble iron fraction.

$$total\ ws\text{-}Fe = Fe^{2+} + Fe^{3+} \quad \text{Eq. 4}$$

This FIA system includes two peristaltic pumps (ISMATEC, IPS 8), a six-port valve (BESTA, Germany) with an injection loop, a two-way switching pinch valve (ASCO S306.02-Z530A), a 2 m reduction coil with an inner diameter of 0.5 mm, an 8 m reaction coil with an inner diameter of 0.5 mm, a UV-Vis light-source (DH-2000-BAL, Ocean Optics, Germany), a USB-Spectrophotometer (USB4000-XR1-ES, Ocean Optics, Germany) and a liquid waveguide capillary cell (LWCC 3100, World

https://doi.org/10.5194/ar-2025-37
Preprint. Discussion started: 12 November 2025

Precision Instruments, Friedberg, Germany, 100 cm pathlength, 250 µL internal volume, 550 µm inner diameter) (see Figure 2). The valve circuit of the six-port valve and the two-way pinch valve were controlled with a microcontroller (Arduino Nano). Software for data acquisition was written in LabView 2017 based on Ocean Optics USB4000 code.

Continuous flow samples of MARS or PILS were collected into injection loops (600 µL for MARS, 400 µL for PILS) - both exceeding at least 1.5 times the volume of the LWCC. Due to different system flow rates (MARS: 0.1 mL min^{-1}. PILS: 0.05 mL min^{-1}), the injection volume of the PILS-FIA-system was chosen to be smaller compared to the MARS-FIA-system. The reduced sample flow also leads to a longer sampling time of 12 min for the PILS system compared to 10 min for the MARS system. The sample solutions were injected into the carrier solution. The carrier flow rate was 1.0 mL min^{-1} for the MARS-FIA and 0.5 $mLmin^{-1}$ for the PILS-FIA. The pH of the carrier steam was adjusted according to the pH of the sample flow (pH 6.5 for MARS, pH 4.5 for PILS). At the first mixing point, hydroxylamine hydrochloride (HA) solution or water was introduced into the carrier via the switching valve (flow ratio carrier: HA/H_2O 10:1). The mixed stream enters the reduction coil, where in the presence of HA Fe(III) is reduced to Fe(II). At the second mixing point, ferrozine is introduced to the sample (flow ratio ferrozine:carrier 1:10) before the whole mixture enters the reaction coil. In previous online systems for Fe(II) detection, ferrozine concentrations around 5 mM were commonly used (e.g. Rastogi et al., 2009; Majestic et al., 2006), typically added to the sample at a 1:10 ratio. In this study, a lower ferrozine concentration of 2.7 mM was sufficient for complete complexion of Fe(II), while also reducing chemical consumption.

Experiments with standard solutions indicated that 95 % of the maximum absorbance of the coloured reaction product was already reached after 70 seconds, allowing short reaction times (~80 s for MARS-FIA and ~160 s for PILS-FIA). Due to the short reaction time, reduction of Fe(III) by ferrozine alone was not observed as has been reported in previous studies (Murray and Gill, 1978). As the pH of the sample flow is not expected to be below pH 4.5, which is in the working range of ferrozine as a complexing agent (Zhang et al., 2001; Stookey, 1970), no buffer was used. After passing the reaction coil, the sample enters the LWCC. To prevent the formation of air bubbles due to outgassing, a PTFE capillary (0.5 mm inner diameter, 350 mm length; Metrohm AG, Germany) was attached to the outlet of the LWCC, as it increases the backpressure within the LWCC. The sample absorbance was determined at λ = 562 nm relative to λ = 700 nm. The average baseline was determined over a 75-second interval, from 2 minutes to 45 seconds before the peak, and subtracted from the signal. Quantification using peak height gave better precision than using peak area and was therefore applied in this study. All values were subsequently corrected for blank measurements.

2.2.3 Calibration and daily maintenance

The FIA system was regularly calibrated with 3–5 Fe(II) standards ranging from 0.5 to 40 µg L^{-1}, freshly diluted from a 1 g L^{-1} acidified stock solution. Daily calibration was performed with a 5 µg L^{-1} Fe(II) standard. While Fe(II) is typically stabilized in 0.01 M HCl (Zhang et al., 2001) due to slower oxidation rate in acidic conditions (Millero et al., 1987), neutral pH standards were used here to match sample conditions and yielded reproducible results. Fe(III) standards were used to assess reduction

https://doi.org/10.5194/ar-2025-37
Preprint. Discussion started: 12 November 2025

efficiency and showed improved stability and reproducibility when acidified to pH 3.5, as Fe(III) hydrolysis occurs at pH >3 while Fe(II) hydrolysis occurs at pH>8 (Langmuir, 1997). An optimum pH range of 4-9 for the Fe-ferrozine-complex formation was stated by Stookey (1970), but calibrating with Fe(II) standards of pH 3.5 gave the same results compared to calibrating with neutral pH, underlining that the ferrozine method also works at pH 3.5. To prevent the accumulation of the Fe-ferrozine complex onto the LWCC wall, the LWCC was daily cleaned with 2 % Hellmanex, methanol and 2 M HCl. FIA tubing was washed with 2 M HCl regularly to prevent the precipitation of iron oxides within the tubing.

2.3 Test experiments and instrument evaluation

2.3.1 Test experiments

Following the development of the FIA system, the setup was connected to MARS and tested during a two-week measurement campaign in June 2024 in Berlin, Germany. The system was deployed inside a measurement container located at the main campus of Technische Universität (TU) Berlin, close to the six-lane road “Straße des 17. Juni.” During the campaign, particle size distributions were measured using an ELPI+ (Dekati, Finland), and equivalent black carbon (BC) concentrations were determined with an aethalometer (MA200, AethLabs, USA). After this initial test campaign, the setup was optimized by adjusting the pH of the extraction medium. A second one-week campaign was conducted in March 2025 on the terrace of an institute building at the TU Berlin campus. This time, a PILS was used as the sampling unit, with an acidified sample flow at pH 4.5. BC concentrations were again measured using the aethalometer MA200. $PM_{2.5}$ concentrations were obtained from the background monitoring stations in districts of Berlin (i.e. Wedding, Neukölln, and Mitte), which are part of the Berlin Air Quality Monitoring Network (BLUME).

2.3.2 Offline measurement

To evaluate the results from the online instruments, filter samples were collected during the test field campaigns in Berlin. Additional filter samples were taken at a contrasting location to assess potential application environments: Mace Head, Ireland (autumn 2024), representing background North Atlantic marine air (O’Connor et al., 2008). As different filter samplers, air volumes, filter types and diameter were used at the different locations, all parameters are listed in Table 2. The filters from Mace Head were stored frozen and transported to Berlin frozen. The filters in Berlin were stored at room temperature and in the dark before extraction.

Iron solubility is strongly influenced by pH – lower pH values lead to increased solubility (Liu and Millero, 2002, 1999). Based on the mean pH values reported by Pye et al. (2020) for 93 studies at 48 European locations between 1988 and 2018, the average pH of cloud water in Europe is approximately 4.5. This value lies within the optimal pH range of the ferrozine method and was therefore selected for comparison with neutral pH (pH 6.5) conditions.

https://doi.org/10.5194/ar-2025-37
Preprint. Discussion started: 12 November 2025

To assess the effect of pH reduction on Fe(II) concentration, filter cuts were extracted in Seradest water at pH 4.5 and at pH 6.5 for1 h in a horizontal shaker. Different cut sizes were used depending on the used particle collector (see Table 2). The extracts were filtered through a 0.45 µm polyamide syringe filter (Chromatographie Handel Mueller, Germany) before they were injected into the FIA-system for ws-Fe(II) and total ws-Fe determination. Samples were directly analysed after extraction to minimize hydrolysis and precipitation of Fe(III) as well as oxidation of Fe(II) to Fe(III).

Extraction time and extraction pH vary across different studies published; for example, Chen and Siefert (2003) report that a maximum concentration of labile Fe was reached after 90 min at pH 4.5. To evaluate extraction efficiency at pH 4.5 for the much shorter extraction times typical of particle-into-liquid sampling units (only a few minutes), filters from the second campaign were extracted for 1, 5, 10 and 30 min. The total ws-Fe concentration was determined directly after extraction using the FIA system, and extraction efficiency was then calculated.

Table 2: Summary of filter sampling parameters at the different locations

Station	Sampling duration	Sampler	Cut-off Diameter	Sampling Volume	Filter	Dimension of Filter Cut [mm]	Extraction volume [mL]
Berlin, Straße des 17. Juni	24 h sampling	Lekel, SEQ 47/50	PM 2.5	2.3 m^3h^{-1}	47 mm, Munktell MK360	Ø 15	3
Berlin, Campus TU Berlin	24 h sampling	Digitel	PM 2.5	30 m^3h^{-1}	150 mm, QM-A, Whatman	Ø 25	5
Mace Head, Ireland	5-10 d sampling	HiVol sampler	PM 1.5	97.2 $m^3 h^{-1}$	slotted filters, Whatman41	30 x 10	5

3 Results and Discussion

3.1. Characteristics of the FIA system

3.1.1 Calibration and limit of quantification

Based on measurements of calibration standards and system blanks, the linear working range, the sensitivity, the limit of detection (LOD) and the limit of quantification (LOQ) of the FIA system were obtained.

A universal calibration curve from 0.5 to 40 μgL^{-1} Fe(II) was determined as an average linear regression of ten individual calibration measurements taken over the course of one year (Table A1), based on measurements performed on different days in the laboratory and under varying conditions in the field, including minor fluctuations in flow rates and changes in pump tubing. The individual linear regression slope values ranged from 0.0206 to 0.0280 ($1/\mu g\,L^{-1}$), with an average of 0.0242 ± 0.0024 ($1/\mu g\,L^{-1}$). The intercept was -0.0023 ± 0.0076 and R^2 was 0.996. The low standard deviation of the slopes (<10 %) demonstrates good reproducibility for calibration slopes, highlighting the robustness of the system under varying operational conditions, and confirming its suitability for field deployment. The calibration with freshly prepared Fe(III) standards resulted in 100 % reduction when the standards were less than a few hours old or acidified to pH 3.5. Using fresh and acidified Fe(III)

https://doi.org/10.5194/ar-2025-37
Preprint. Discussion started: 12 November 2025

standards is essential for reliable calibration due to the instability of Fe(III) species at pH > 3 (see Section 2.2.3). A decrease in reduction efficiency was observed with increasing age of the Fe(III) standards. This observation highlights that, under the short reduction times in the FIA system, less reactive or less reducible Fe(III) species may not be fully reduced. To acknowledge this limitation imposed by the operational reduction time, we therefore use further on the term reducible Fe(III) instead of ws-Fe(III).

The average blank concentrations from the test field campaigns (n=2) are listed in Table 1. Generally, the mean blank concentrations of total soluble Fe (MARS-FIA: 1.84 ngm^{-3}, PILS-FIA: 3.51 ngm^{-3}) are higher compared to the mean blank concentrations of Fe(II) (MARS-FIA: 1.01 ngm^{-3}, PILS-FIA: 0.84 ngm^{-3}). The PILS-FIA-system shows higher blank values for total soluble iron than the MARS-FIA system. An advantage of the MARS is the fast and simple washing procedure, as the SJAC can quickly be dismantled and cleaned in isopropanol in an ultrasonic bath.

The lowest LOD with 0.15 ngm^{-3} was determined for total ws-Fe using the PILS-FIA setup (Table 1). The highest LOD with 0.48 ngm^{-3} (Table 1) was determined for total ws-Fe using the MARS-FIA setup. The LOQ from the blank measurement of total soluble Fe was 1.6 ngm^{-3} for the MARS-FIA and 1.0 ngm^{-3} for the PILS-FIA (Table 1). The blank uncorrected LOQ for the MARS-FIA system was 2.7 ngm^{-3}, which corresponds to 0.45 μgL^{-1}, and 5.1 ngm^{-3} for the PILS-FIA system, which corresponds to 1.15 μgL^{-1}. These liquid concentrations are at the lower end of the calibration range.

3.1.2 Effect of pH and extraction time

As iron solubility is directly influenced by pH, which typically ranges between 3 and 6 in cloud water (Pye et al., 2020), filters were extracted at near-neutral pH (6.5) and slightly acidic pH (4.5) (see section 2.3.2).

At pH 6.5, the lowest ws-Fe concentrations were found at Mace Head, Ireland (Table 3, Filters C1–C5), with ws-Fe(II) ranging from <LOQ to 0.04 ng m^{-3}. Total ws-Fe concentrations were only slightly higher (LOQ–0.06 ng m^{-3}), resulting in ws-Fe(II)/total ws-Fe ratios around 0.8. These high ratios indicate that nearly all soluble iron was present as Fe(II).

When extracted at pH 4.5, both ws-Fe(II) and total ws-Fe concentrations increased, reaching 0.07–0.16 ng m^{-3} and 0.13–0.29 ng m^{-3}, respectively. The relative increase was higher for total ws-Fe than for ws-Fe(II), leading to a lower ws-Fe(II)/total ws-Fe ratio of 0.45–0.70. This indicates that under slightly acidic conditions, more reducible Fe(III) compounds dissolved than Fe(II), as expected from the enhanced solubility of Fe(III) oxides and Fe(III) hydroxides at lower pH (e.g. Balsamo Crespo et al., 2023; Langmuir, 1997; Pye et al., 2020). The very low ws-Fe(II) and total ws-Fe concentrations evidence the clean air and pristine marine conditions at Mace Head.

In contrast to the clean marine air masses sampled at Mace Head, Berlin urban air is strongly influenced by anthropogenic activity, which is reflected in higher concentrations of both ws-Fe(II) and total ws-Fe (Table 3). During the second test campaign in winter 2025 (Filters B5–B9), extraction at pH 6.5 yielded ws-Fe(II) concentrations between 1.1 and 7.5 ng m^{-3} and total ws-Fe between 3.2 and 16.47 ng m^{-3}. The resulting ws-Fe(II)/total ws-Fe ratios of 0.22–0.46 indicate that a large fraction of soluble Fe was present as reducible Fe(III) rather than Fe(II). When filters were extracted for 1 h at pH 4.5,

https://doi.org/10.5194/ar-2025-37
Preprint. Discussion started: 12 November 2025

concentrations increased substantially: ws-Fe(II) increased to 10.78–21.63 ng m^{-3} and total ws-Fe to 11.76–25.47 ng m^{-3}. This acid-driven increase in both species resulted in higher ws-Fe(II)/total ws-Fe ratios of 0.68–0.92, suggesting that in Berlin aerosol particles a significant proportion of soluble Fe at low pH is Fe(II), likely due to Fe(II)-rich phases, Fe(III) reduction, and or stabilization of Fe(II) by complexing agents like oxalate (Giorio et al., 2025) .

The speciation between ws-Fe(II) and Fe(III) in ambient atmospheric particles has been investigated in several studies before (e.g. Gao et al., 2019, 2020; Kuang et al., 2017; Majestic et al., 2006). This speciation is useful for identifying sources of water-soluble iron in dust because the ws-Fe(II)/ws-Fe(III) ratio varies according to origin. For instance, previous studies have revealed that diesel exhaust particles typically exhibit low water-soluble Fe(II)/Fe(III) ratios (Valavanidis et al., 2000), whereas particles originating from biomass burning exhibit notably higher ratios (Wang et al., 2022; Fu et al., 2012). Our extracted filters further show that iron solubility and speciation are strongly influenced by pH. The observation aligns with findings of Majestic et al. (2006), observing that ws-Fe(II) to reducible Fe(III) ratios vary between extractions performed with Milli-Q water (pH 6.3) and those with acetate buffer (pH 4.3). This suggests that iron sources could be identified by determining the dissolved Fe species under different conditions. Therefore, it is important to consider pH dependence when comparing Fe(II)/Fe(III) speciation data from different studies.

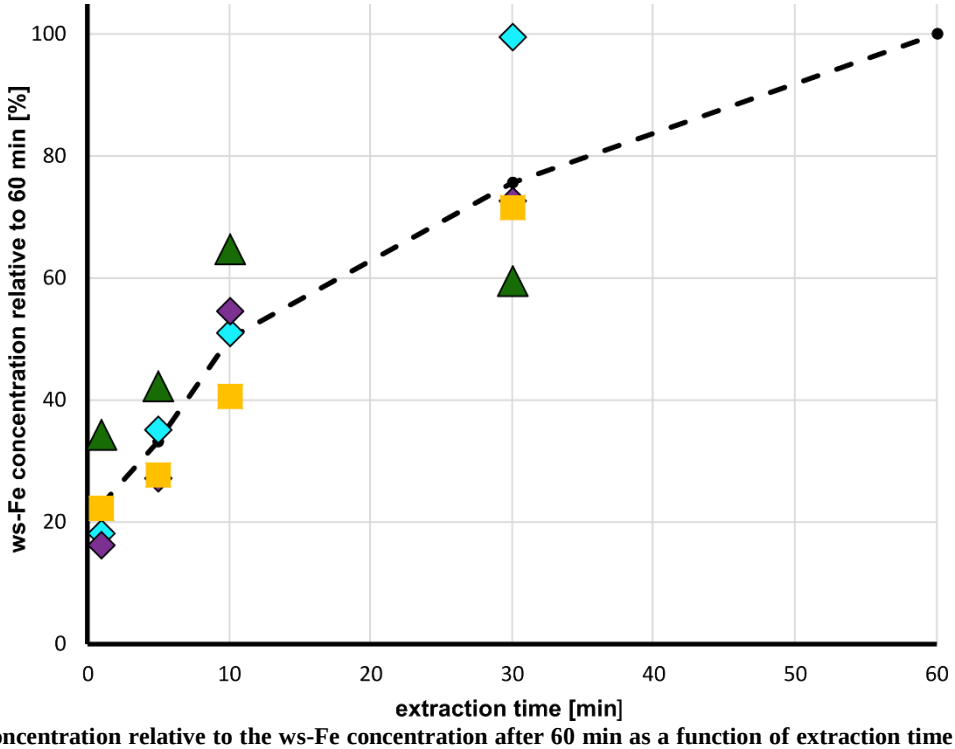

Figure 3: ws-Fe concentration relative to the ws-Fe concentration after 60 min as a function of extraction time for four filters (B5-B8) from the second field campaign. The filters were extracted in pH 4.5 solution and total ws-Fe was determined. Coloured symbols represent the efficiencies determined for the four different filter samples (B5-B8); the black dashed line indicates the average.

https://doi.org/10.5194/ar-2025-37
Preprint. Discussion started: 12 November 2025

The extraction times within the MARS-FIA and PILS-FIA systems were shorter than in the 1 h offline filter extraction procedure. Particles not dissolved during sampling can remain suspended in the liquid stream if filtration is not applied. In the MARS-FIA setup, the liquid sample passed through a 0.45 µm syringe filter before entering the FIA system, whereas no filter was used in the PILS-FIA setup. In both setups, the transfer time from the sampling unit to the FIA system was approximately 2 min. The sampling time into the injection loop was 10 min for the MARS-FIA and 12 min for the PILS-FIA (Table 1) guaranteeing a complete filling of the injection loop with sample. After injection, the total residence time of the sample in the FIA system was 1 min 45 s for MARS-FIA and 3 min 30 s for PILS-FIA. Therefore, the total time that particles were in contact with the liquid phase was about 14 min in MARS-FIA and 18 min in PILS-FIA. To investigate the efficiency of extraction as a function of extraction time, filters from the second test campaign (filters B5-B8) were also analysed after 1, 5, 10 and 30 min of extraction at pH 4.5. The results are listed in Table A2, and the extraction efficiency, normalized to the concentration obtained after 1 h of extraction, is shown as a function of time in Figure 3. The coloured symbols represent the efficiencies determined for the four different filter samples, while the black dashed line indicates their average. After 1 min of extraction, only 20–30 % of the total ws-Fe was dissolved. After 10 min, the extracted fraction increased to 40–60 %. After 30 min, filter B7 (turquoise squares) already reached complete extraction relative to the 1 h filter extraction, whereas the efficiencies for the other three filters remained between 60 and 70 % (Figure 3).

Overall, these results show, that the extraction time is an important factor when determining the concentration of ws-Fe at slightly acidic conditions. As the extraction time in the online instruments is shorter compared to filter analysis, the concentration determined online might not represent the total extractable ws-Fe. Therefore, extraction time is an important factor to consider when comparing measurements and interpretations between different studies.

3.2. Test campaigns and first field application

Concentrations of ws-Fe(II) and total ws-Fe were measured with the online system and with offline filter samples during two test campaigns in Berlin, at *Straße des 17. Juni* in June 2024 and on the main campus of TU Berlin in March 2025.

3.2.1 Comparison of online and offline measurements

The concentrations of water-soluble Fe(II) (ws-Fe(II), light-red) and total water-soluble Fe (total ws-Fe, dark-red) measured online during the two test campaigns are shown in Figure 4. Shaded areas indicate values obtained from offline filter analysis. During the first campaign at *Straße des 17. Juni* in June 2024, online ws-Fe(II) and total ws-Fe concentrations varied between 1 and 9 ng m^{-3}, except between 08.06.2024 and 09.06.2024, when total ws-Fe reached 50 ngm^{-3} (Figure 4a). On average, during the period the online ws-Fe concentration was 5.2 ngm^{-3}. Elevated soluble Fe concentrations during this period of the first campaign were also observed in the offline filter samples, with an average offline ws-Fe(II) concentration of 17.0 ngm^{-3} on 08.06.2024 (Table 3, Filter A4). Averaged online ws-Fe(II) concentrations from the MARS-FIA system for the corresponding period were 19.5 ngm^{-3}.

https://doi.org/10.5194/ar-2025-37
Preprint. Discussion started: 12 November 2025

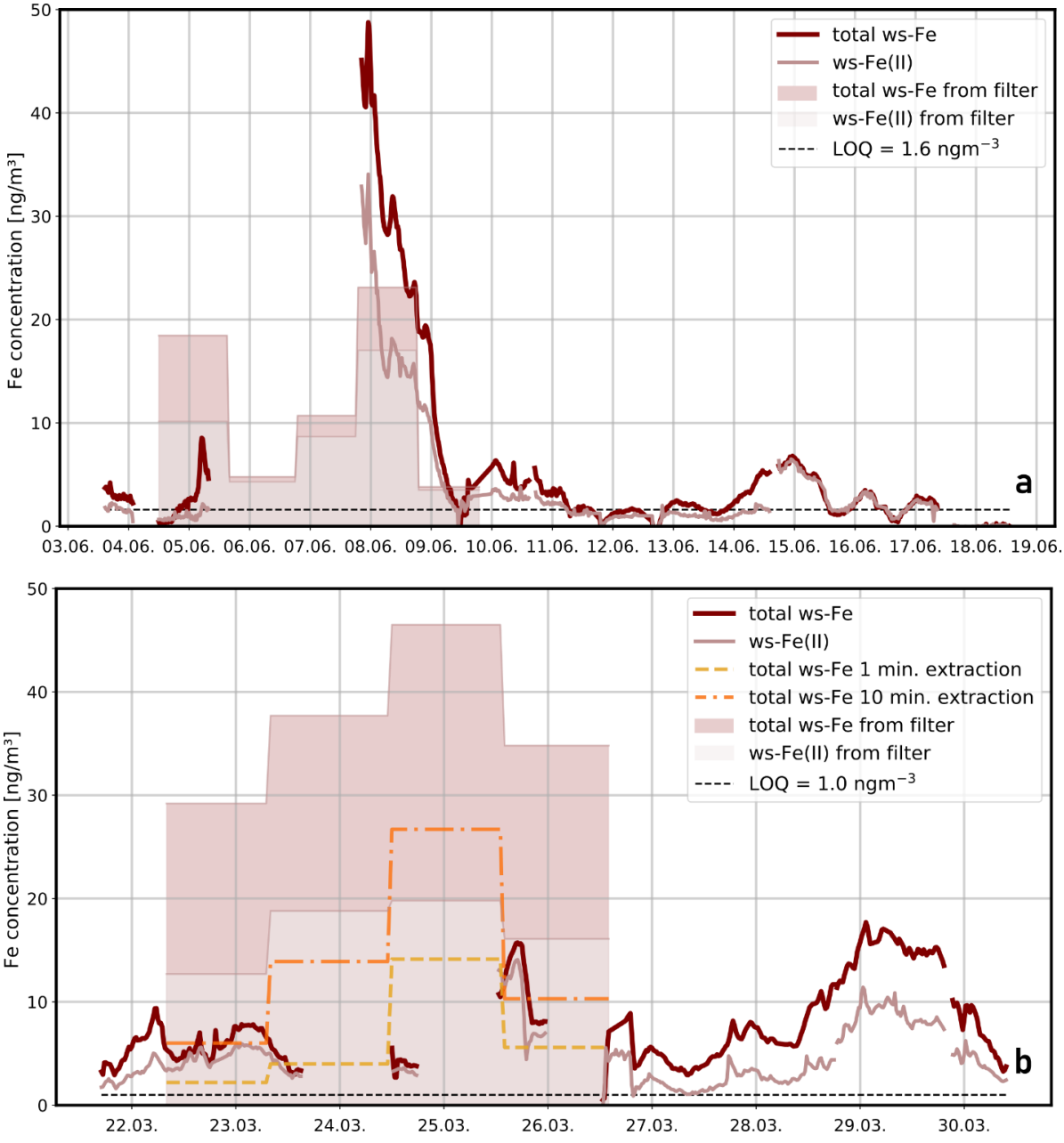

Figure 4: Temporal variability of total ws-Fe (red) and ws-Fe(II) (light-red) concentrations in particulate matter (PM2.5) in Berlin: a) First test campaign with MARS-FIA setup at the road *Straße des 17. Juni* from 03.06.-19.06.2024. The shaded areas represent the concentrations obtained by filter analysis with filter extraction in Seradest water. The black dashed line represents the LOQ from blank measurements. b) Second test campaign with PILS-FIA setup at TU Berlin Campus from 22.03.-30.30.2025. The shaded areas represent the concentrations obtained by filter analysis with extraction at pH 4.5. The dashed yellow line represents the concentrations from 1-min-filter extraction at pH 4.5. The dashed orange line represents the concentrations after 10-min-filter extraction at pH 4.5. The black dashed line represents the LOQ from blank measurements.

https://doi.org/10.5194/ar-2025-37
Preprint. Discussion started: 12 November 2025

345

Table 3: Offline ws-Fe(II) and total ws-Fe concentrations from filter extraction. Filters were extracted for 1 h in pure Seradest water with pH 6.5 and with acidified Seradest water with pH 4.5

ID	Location	Date	ws-Fe(II) [ng/m^{-3}] pH 6.5	total ws-Fe [ng/m^{-3}] pH 6.5	ws-Fe(II)/ total ws-Fe [-] pH 6.5	ws-Fe(II) [ng/m^{-3}] pH 4.5	total ws-Fe [ng/m^{-3}] pH 4.5	ws-Fe(II)/ total ws-Fe [-] pH 4.5	ws-Fe(II) $_{pH\ 4.5}$/ ws-Fe(II) $_{pH\ 6.5}$ [-] pH 4.5/pH6.5	total ws-Fe $_{pH\ 4.5}$ / total ws-Fe $_{pH\ 6.5}$ [-] pH 4.5/pH6.5
A1	Berlin, Str. 17. J	04.06.-05.06.2024	10.1	18.5	0.5	n.a.	n.a.	n.a.	n.a.	n.a.
A2	Berlin, Str. 17. J	05.06.-06.06.2024	2.9	4.8	0.6	n.a.	n.a.	n.a.	n.a.	n.a.
A3	Berlin, Str. 17. J	06.06.-07.06.2024	8.7	10.7	0.	n.a.	n.a.	n.a.	n.a.	n.a.
A4	Berlin, Str. 17. J	07.06.-08.06.2024	17.0	23.1	0.72	n.a.	n.a.	n.a.	n.a.	n.a.
A5	Berlin, Str. 17. J	08.06.-09.06.2024	2.4	3.1	0.8	n.a.	n.a.	n.a.	n.a.	n.a.
B1	Berlin, TUB	03.06.-05.06.2024	5.1	n.a.	n.a.	n.a	n.a	n.a	n.a.	n.a
B2	Berlin, TUB	05.06.-07.06.2024	2.4	n.a.	n.a	n.a	n.a .	n.a	n.a.	n.a
B3	Berlin, TUB	10.06.-12.06.2024	0.3	n.a.	n.a	n.a	n.a .	n.a	n.a	n.a
B4	Berlin, TUB	12.06.-14.06.2024	0.1	n.a.	n.a	n.a	n.a	n.a	n.a.	n.a
B5	Berlin, TUB	22.03.-23.03.2025	1.1	3.2	0.3	10.8	11.8	0.92	9.80	3.68
B6	Berlin, TUB	23.03.-24.03.2025	2.9	7.3	0.4	21.6	25.5	0.85	7.46	3.47
B7	Berlin, TUB	24.03.-25.03.2025	7.5	16.5	0.5	34.5	41.5	0.83	4.60	2.52
B8	Berlin, TUB	25.03.-26.03.2025	5.5	18.2	0.2	17.4	25.5	0.68	3.16	1.03
C1	MH, Ireland	16.10-23.10.2024	< LOQ	< LOQ	n.a.	0.07	0.23	0.29	n.a.	n.a.
C2	MH, Ireland	14.11.-19.11.2024	0.04	0.06	0.81	0.13	0.29	0.45	2.9	5.2
C3	MH, Ireland	19.11.-27.11.2024	0.03	0.04	0.79	0.09	0.16	0.57	2.7	3.8
C4	MH, Ireland	27.11.-05.12.2024	0.02	0.03	0.80	0.07	0.13	0.50	2.7	4.2
C5	MH, Ireland	10.12.-19.12.2024	0.04	0.05	0.80	0.16	0.24	0.70	4.4	5.1

* n.a.: no data available

On 09.06.2024, ws-Fe(II) concentrations decreased rapidly to values below the limit of quantification. Filter-based ws-Fe(II) was 2.4 ngm^{-3} (Table 3, Filter A5), while the online MARS-FIA system measured an average of 5.0 ngm^{-3}. These results
350 demonstrate a good agreement between online and offline measurements. The total ws-Fe concentrations for 08.06.2024 and 09.06.2024, determined from filter analysis, 23.1 ng m^{-3} and 3.1 ng m^{-3}, respectively (Table 3, Filter A4 & A5), while average total ws-Fe concentrations from the online MARS-FIA system were higher, i.e. 31.7 ngm^{-3} and 7.6 ngm^{-3}, respectively. The total ws-Fe concentrations measured by MARS-FIA are thus substantially higher compared to the filter analysis. Both, Fe(II) and Fe(III) ions are not stable in water at pH 6.5. On the one hand, ws-Fe(II) quickly oxidizes to Fe(III). Pham and Waite
355 (2008) found a half-life time for the oxidation of 50 nM Fe(II) of approximately 5 h at pH 6, which increases with increasing pH. Furthermore, ws- Fe(III) rapidly hydrolyses to form $Fe(OH)^{2+}$ and can subsequently undergo further hydrolysis and precipitation. Extraction for 1 h in Seradest water at pH 6.5 may therefore result in both oxidation of Fe(II) and hydrolysis and precipitation of Fe(III). Potentially, this could result in an insufficient reduction time of HA in the FIA system to fully reduce Fe(III) back to Fe(II) as it was observed with aged Fe(III) standards (see section 3.1.1), leading to lower measured total ws-Fe
360 concentrations compared to the online MARS-FIA system, where the sample is analysed within minutes and therefore less oxidation, hydrolysis and precipitation can be expected.

The temporal variability of ws-Fe(II) and total ws-Fe concentrations during the field campaign with the PILS-FIA setup at the Campus of TU Berlin is illustrated in Figure 4b. The concentration of total ws-Fe ranges between 1.0 and 17.7 ngm^{-3} and thus not higher compared to the first field campaign even though the sample flow of the PILS-FIA setup was acidified to pH 4.5
365 (see section 2.2.1). In the period of 22.03. to 26.03.2025, 24 h-filters were collected (Table 3, Filters B5-8). To match the pH of extraction solution and wash flow from PILS, the filters were extracted at pH 4.5 and extracted with different extraction

https://doi.org/10.5194/ar-2025-37
Preprint. Discussion started: 12 November 2025

times (see section 2.3.2). The shaded areas represent the concentrations determined for 1h-extraction time at pH 4.5. As highlighted in Figure 4b, the concentrations for both ws-Fe(II) and total ws-Fe determined are more than twice as high as those determined by the online PILS-FIA. A comparison of the concentration measured by PILS-FIA with those from the filters extracted for 1 min (yellow dashed line) and 10 min (orange dashed line, Figure 4b) shows that 1-minute extraction concentrations are lower than the online concentrations, while those after 10 min extraction fit well with concentrations determined with the online PILS-FIA setup. Due to missing PILS-FIA data from the evening of 24.03.2025 until the morning of 26.03.2025, only two filters (B5 & B8) can be compared with the online concentrations. The average concentrations determined with the PILS-FIA during the sampling period of filter B5 and B8 were 6.0 ngm^{-3} and 10.6 ngm^{-3}, respectively. When comparing these concentrations with the concentrations after 1, 5, 10 and 30 min of extraction (Table A2), the concentrations after 10 min of extraction, i.e. 6.0 and 13.9 ngm^{-3}, respectively, show very good agreement with the PILS-FIA measurement where the total residence time of the sample is around 17 min and 30 s (see section 3.1.2).

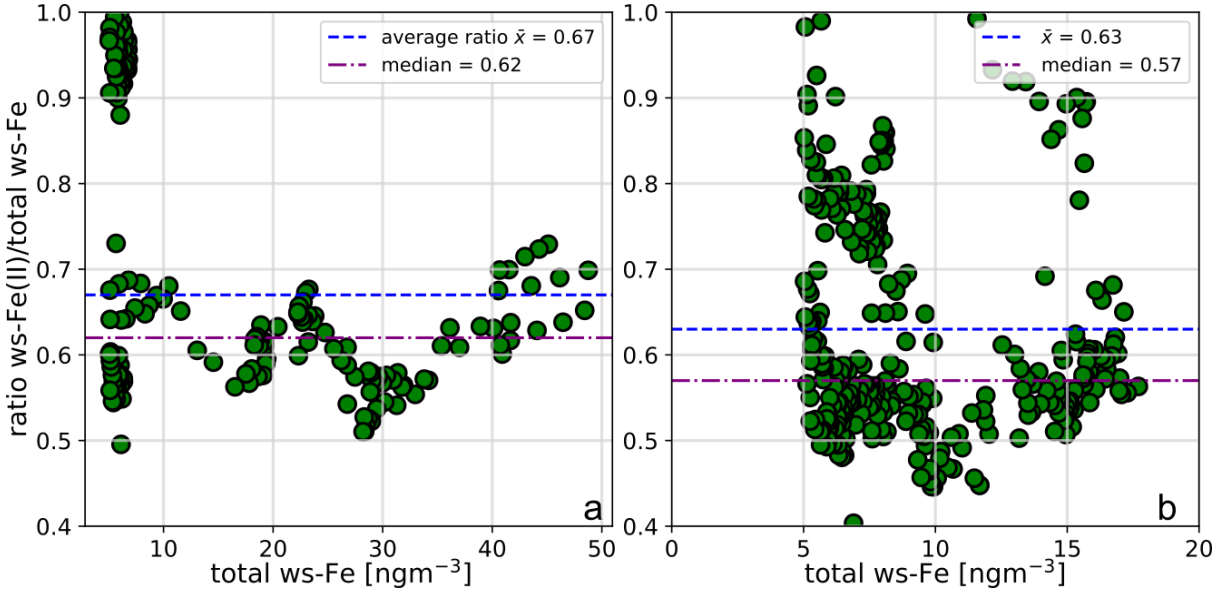

Figure 5: Ratios of ws-Fe(II)/total ws-Fe concentration over total ws-Fe concentration > 5ngm^{-3} during a) the field test campaign at *Straße des 17. Juni in June 2024 and* b) on the campus of TU Berlin in March 2025.

The ratio between ws-Fe(II) and total ws-Fe of the online system in relation to the total ws-Fe concentrations > 5ngm^{-3} is shown in Figure 5. Total ws-Fe concentrations > 5 ngm^{-3} were chosen due to an increased relative error when calculating the ratios for lower total ws-Fe and ws-Fe(II) concentrations. The ratios during the summer test campaign with the MARS-FIA vary between mostly 0.5 and 0.7 resulting in an arithmetic mean of 0.66 and a median of 0.62 (Figure 5a).

The ratios during the winter test campaign with the PILS-FIA show higher variability compared to the first MARS-FIA test campaign ranging from 0.4 to 1.0 resulting in an arithmetic mean of 0.63 and a median of 0.57 (Figure 5b). The ws-Fe(II) to total ws-Fe ratio of the filter samples is listed in Table 3. The ratios from filter analysis from the MARS-FIA vary between

https://doi.org/10.5194/ar-2025-37
Preprint. Discussion started: 12 November 2025

0.55 and 0.81 resulting in an arithmetic mean of 0.69, thus being slightly higher compared to the ratios determined with the online system. The higher ws-Fe(II) to total ws-Fe ratios from the filter samples compared to the ratio determined by MARS-FIA again reflect lower concentrations of total ws-Fe in offline filter analysis compared to the online system as discussed above.

The arithmetic mean of the ratios of the four filters from the PILS-FIA test campaign, which were extracted at pH4.5 for 1 h, is 0.82 and thus significantly higher compared to the mean ratio determined from the PILS-FIA online concentrations, which is 0.63 and thus similar to the first test campaign (MARS-FIA with Seradest). While the ratios between the first and second field campaigns determined online were similar, even though they were conducted at different extraction pH, the ratios ws-Fe(II)/total ws-Fe from the filter extractions differ markedly between the two campaigns. The filter ratio from the first campaign (extracted with Seradest water at pH 6.5) is 0.61, while that from the second campaign (extracted at pH 4.5) is 0.82. This difference, comparable online ratios versus divergent offline ratios, highlights the influence of extraction time within the online system, which appears to have an higher impact than acidification of the sample flow.
In general, no temporal difference in the ratios observed during day and night could be identified (see Figure A1). In a study by Majestic et al. (2006) filter samples from an urban station in St. Louis (August 2004) were extracted with different leachates, and the ws-Fe(II) and total ws-Fe concentrations were determined using the ferrozine method. In their study, ws-Fe concentrations ranged from 5 to 25 ng m^{-3}, depending on the leachate used, resulting in ws-Fe(II) to total ws-Fe ratios of 0.5 to 0.6. The ws-Fe(II) and total ws-Fe concentrations determined by both the MARS- and PILS-FIA setups in this study are therefore consistent with previous work on ws-Fe in urban environments.

3.2.2 Comparison of ws-Fe with PM2.5 and black carbon (BC)

During the first field campaign in June 2024, the MARS-FIA setup was placed close to the main artery *road Straße des 17. Juni* in Berlin city centre, thus measuring air which is highly influenced by traffic. Particle size distributions and BC concentrations were also measured (see section 2.3.1). The temporal variability of $PM_{2.5}$ (light-blue) and total ws-Fe (dark red) is illustrated in Figure 6a. The $PM_{2.5}$ concentrations varied between 2 and 47 µgm^{-3} resulting in an average of 14 µgm^{-3}. The total ws-Fe concentrations were three orders of magnitude lower, following the trend of the $PM_{2.5}$ concentrations. Between 07.06. and 08.06.2024 the $PM_{2.5}$ concentration remained relatively high around 30 µgm^{-3}. Data for the 07.06.2024 are missing from the PILS-FIA system but the highest total ws-Fe concentrations measured during the period were between 40 and 50 ng m^{-3} on 08.06.2024. reaching a maximum with 48.7 ng m^{-3} when also $PM_{2.5}$ concentrations were high. In the night of 09.06.2024 both concentrations dropped rapidly, before they rose again on 10.06.2024. On 14.06.2024, $PM_{2.5}$ again reached concentrations close to 40 µg m^{-3}. Total ws-Fe concentrations also increase during that time reaching a maximum of 6.8 ng m^{-3} at 23:20 of 14.06.2024. For the linear regression between $PM_{2.5}$ and total ws-Fe concentrations, a Pearson correlation coefficient of 0.49 indicates a moderate correlation ($p < 3.4 \cdot 10^{-47}$). Plotting the $PM_{2.5}$ concentration against the total ws-Fe

https://doi.org/10.5194/ar-2025-37
Preprint. Discussion started: 12 November 2025

concentration (Figure 7a), two distinct groups of data points appear to form. The total ws-Fe concentrations higher than 15 ngm^{-3}, measured on 08.06.2024 and highlighted in beige in Figure 7a, stand apart from the total ws-Fe concentrations below 15 ngm^{-3} from the rest of the campaign, shown in brown colour. Focusing on the lower total ws-Fe concentrations (< 15 ngm^{-3}) in Figure 7b, these values correspond to a mass fraction of total ws-Fe between 0.15 and 2 ‰ of $PM_{2.5}$, with most mass fractions falling between 0.15 and 0.3 ‰. Contrary to the low total ws-Fe concentrations, the high total ws-Fe concentrations (>15 ngm^{-3}) converge at a mass fraction of 2 ‰ of $PM_{2.5}$.

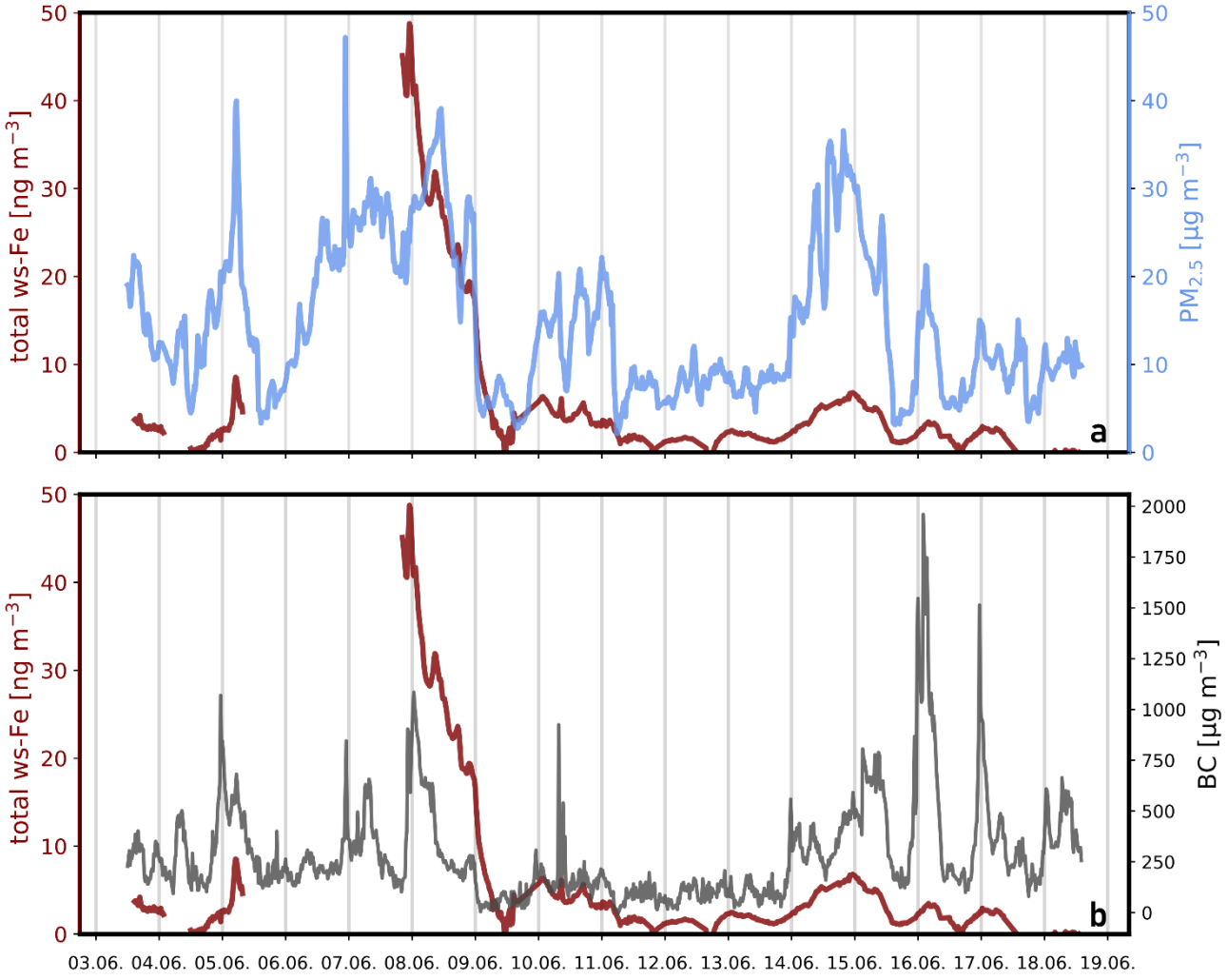

Figure 6: Temporal variability of total ws-Fe and PM2.5 (a) and total ws-Fe and BC(b) during the first test campaign at *Straße des 17. Juni* in June 2024.

https://doi.org/10.5194/ar-2025-37
Preprint. Discussion started: 12 November 2025

Salazar et al. (2020a) reported an average water-soluble iron concentration of 7.7 ng/m³ in downtown Denver aerosols sampled during both summer and winter, corresponding to an average water-soluble iron fraction of approximately 4.2% of total iron. Crazzolara and Held (2024) measured a contribution of total iron in PM10 ranging from 1.4 to 3.7% during a one-day measurement campaign in Berlin city centre. Assuming a total iron content of 1–4% in $PM_{2.5}$ and an iron solubility of 3–5%, the expected total ws-Fe concentration would range from approximately 0.3 to 2‰ of the total $PM_{2.5}$ mass. This is consistent with our measurements and evidences the plausibility of the data. The elevated concentrations on 08.06.204 may either reflect generally high total iron levels or indicate an emission event specifically rich in water-soluble iron.

The ratio between ws-Fe(II) and total ws-Fe on 08.06.2024 was 0.59, which is slightly lower compared to the arithmetic mean value of 0.67 in the campaign, indicating increased emissions of reducible Fe(III) compared to ws-Fe(II) on 08.06.2024.

The temporal variability of BC (grey) and total ws-Fe concentrations is illustrated in Figure 6b. The concentration of BC varies between LOD and 2 µg m^{-3} reaching its maximum on 16.06.2024. For the linear regression between BC and total ws-Fe concentrations, a Pearson correlation coefficient of 0.35 ($p < 1.87 \cdot 10^{-23}$) indicates a weaker correlation for BC compared to the $PM_{2.5}$ concentrations. On 08.06.2024, when total ws-Fe concentrations were high (>15 ngm^{-3}), BC concentrations were also elevated (see Figure A2) indicating an emission event that could be related to combustion processes such as traffic. ws-Fe concentrations originating from vehicle exhaust were investigated by Salazar et al., 2020b. They demonstrated that ws-Fe is formed through the dissolution of iron in water mediated by specific organic compounds present in the exhaust. The authors proposed that anthropogenic ws-Fe mainly results from chelation with these organic compounds or their likely aqueous reaction products.

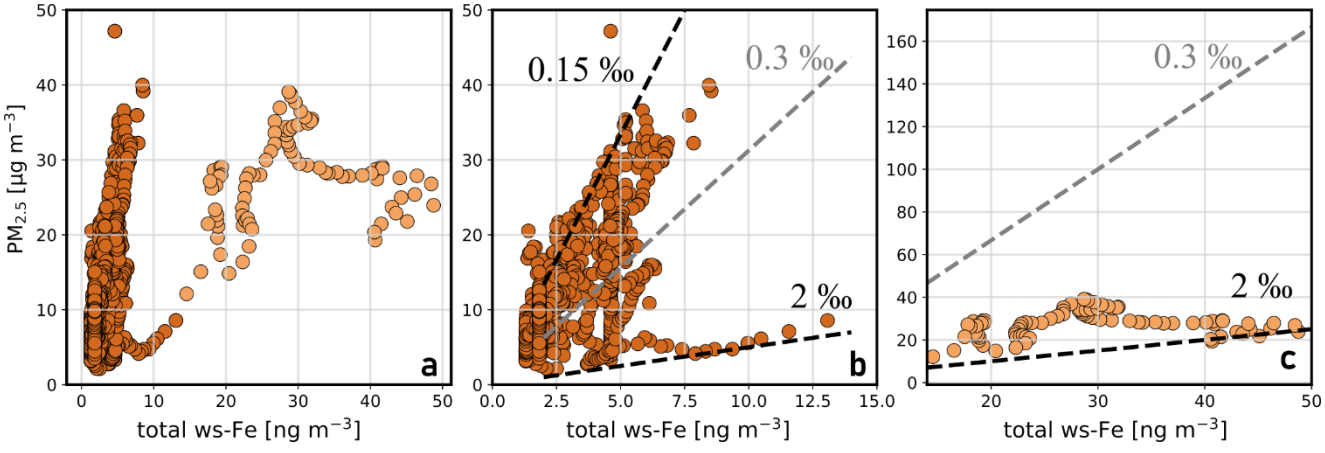

Figure 7: Relationship between $PM_{2.5}$ concentration and total ws-Fe concentration from the MARS-FIA test campaign in June 2024. (a) Scatter plot of all data points. $PM_{2.5}$ concentrations where the corresponding total ws-Fe concentration is < 15 ngm^{-3} are shown in brown. Those were total ws-Fe is > 15 ngm^{-3} are presented in beige (b) Scatter plot of $PM_{2.5}$ versus total ws-Fe concentration <15 ngm^{-3}. The dashed lines correspond to Fe mass fractions of 2 ‰ ,0.3 ‰ and 0.15 ‰, illustrating the range of mass fractions of ws-Fe in $PM_{2.5}$ observed during the campaign. (c) Scatter plot of $PM_{2.5}$ versus total ws-Fe concentration >15 ngm^{-3}, illustrating the mass fraction of total ws-Fe in $PM_{2.5}$ tends towards 2 ‰ for these concentration levels. Note the different scales in 7 (c).

https://doi.org/10.5194/ar-2025-37
Preprint. Discussion started: 12 November 2025

The second field campaign was conducted in March 2025 on the TU Berlin campus with the PILS-FIA setup with a sample flow pH of 4.5. During this period, air quality in Berlin ranged from moderate to poor, as indicated by $PM_{2.5}$ concentrations at the Berlin background stations, which ranged up to 40 μgm^{-3} and averaged 20 μgm^{-3} over nine days (see Figure A3). In contrast, the average $PM_{2.5}$ concentration during the first field campaign was only 8 μgm^{-3}. The mean total ws-Fe concentration was 7.0 ngm^{-3}, marginally higher than in the first campaign. Additionally, the variability in total ws-Fe concentrations was lower than previously observed, ranging from 2.7 to 17.2 ngm^{-3}. The temporal patterns of both total ws-Fe (dark red) and $PM_{2.5}$ (light blue), as well as total ws-Fe and black carbon (BC) concentrations (grey), are shown in Figure A4. As in the first field campaign, total ws-Fe trends followed both the $PM_{2.5}$ and BC concentrations. The ratio of total ws-Fe to $PM_{2.5}$ was consistent with the first campaign, ranging between 0.15 and 2 ‰ (see Figure A4a). The Pearson correlation coefficient between total ws-Fe concentrations >5 ng m^{-3} and $PM_{2.5}$ was 0.25 ($p < 0.004$), indicating a weak correlation. Similarly, a weak correlation was observed between total ws-Fe concentrations >5 ng m^{-3} and BC concentrations <800 μgm^{-3} (Pearson $r = 0.28$, $p < 1.6\times10^{-5}$).

The average ratio of ws-Fe(II) to total ws-Fe for concentrations above 5 ngm^{-3} was 0.63, only slightly lower than in the first campaign (see Figure 5).

Overall, the second campaign, conducted in winter 2025 at the campus of TU Berlin, showed total ws-Fe concentrations comparable to the first campaign in summer (June 2024 at *Straße des 17. Juni*) thus indicating no clear seasonal difference even though the $PM_{2.5}$ concentrations of the background stations were notably higher during the winter test campaign. Salazar et al. (2020a) investigated ws-Fe concentrations at three locations, which were defined as 1) urban, 2) rural and agriculture and 3) urban and agriculture in summer and winter of 2016 and 2017. Across all three sites they observed that ws-Fe concentrations were lower in winter, even though total iron concentrations were higher during that season. The ws-Fe concentrations between the sampling week in March 2025 and the nearly three weeks of sampling in June 2025 show comparable levels even though they represent different seasons. The fact, that no seasonal difference was observed could be the results of comparing two different sites with each other during different seasons which are close to each other but differently affected by traffic. However, the results of the second test campaign underline that the slightly acidic wash flow of pH 4.5 used in the PILS-FIA setup does not significantly affect iron's solubility or oxidation state during sampling compared to sampling in MARS with pH 6.5.

4. Suitability of the FIA System for Field Measurements

Both field test campaigns demonstrate that the developed FIA system, designed for near real-time measurement of ws-Fe(II) and total ws-Fe concentrations in particulate matter, can be effectively used in combination with the MARS and PILS sampling units in an urban environment. The system is suitable for urban environments where total ws-Fe concentrations exceed 1 ng m^{-3}. To assess its applicability in different environmental conditions, filter samples were collected at Mace Head, Ireland,

https://doi.org/10.5194/ar-2025-37
Preprint. Discussion started: 12 November 2025

as described in section 2.3.2. Because Mace Head represents a pristine environment with expectedly low iron concentrations, filter sampling with a sampling periods between 5 and 10 days was performed. Results shown in Table 3 indicate very low total ws-Fe concentrations - ranging from <LOQ to 0.05 ng m^{-3} - when extracted with Seradest water at pH 6.5. These findings illustrate the substantially lower iron solubility in regions with minimal anthropogenic emissions. Even after acidifying the extraction solution to pH 4.5, total ws-Fe concentrations ranged between 0.13-0.29 ng m^{-3}, thus still remaining below 1 ng m^{-3}. For application at remote sites with total ws-Fe concentrations below 1 ng m^{-3}, the LOQs of both the MARS-FIA and PILS-FIA setups, given their current settings, are too high to reliably detect near real-time ws-Fe concentrations. Further acidification of the wash flow to pH 2 or 3 is unlikely to sufficiently boost ws-Fe concentrations due to the short extraction times available. Therefore, quantification of ws-Fe in remote locations would require methodological adaptations, such as pre-concentration, increasing extraction time within the sampling unit, extending residence time in the online apparatus before ferrozine addition, or increasing the ratio of gas volume to volume of extractant through collecting larger air sample volumes. Nevertheless, the FIA system was successfully applied in two field campaigns in Berlin, and provides speciation capability of water-soluble iron in ambient aerosols in future field measurements, especially in urban and semi-urban environments.

Acknowledgements

We gratefully acknowledge funding from the ATMO-ACCESS project, which has received funding from the European Union's Horizon 2020 Research and Innovation Framework Programme (H2020-INFRAIA).

Access to the Mace Head Atmospheric Research Station for the FeNTASI project was provided through the ACTRIS Trans-National Access (TNA) programme (project ID: ATMO-TNA-5G--0000000065). Further, we would like to thank Metrohm Process Analytics for providing the MARS system and especially Kerstin Dreblow and Jerry van Bronckhorst for their invaluable support with the MARS system.

Author Contributions

S.L.: Conceptualization, Methodology, Software, Validation, Formal Analysis, Investigation, Writing-Original Draft, S.K: Methodology, Conceptualization, Investigation, F.F.: Methodology, Software, D.C.: Investigation, Resources, Writing-Review & Editing, D.v.P.: Resources, Writing-Review & Editing, H.H.: Resources, Writing-Review & Editing, A.H.: Conceptualization, Software, Resources, Writing-Review & Editing.

Competing interests

A.H. is a member of the editorial board of *Aerosol Research*.

https://doi.org/10.5194/ar-2025-37
Preprint. Discussion started: 12 November 2025

AEROSOL Research Discussions

Appendix

Table A1: Results of linear regression from calibration over one year

Date	a	b	R^2	pH
08.04.2024	0.0244	-0.0050	0.9997	6.5
09.04.2024	0.0255	-0.0019	0.9955	6.5
11.04.2024	0.0246	-0.0015	0.9977	6.5
14.02.2024	0.0224	-0.0014	0.9951	6.5
28.05.2024	0.0252	-0.0193	0.9983	6.5
10.11.2024	0.0222	-0.0025	0.9999	3.5
13.02.2025	0.0206	-0.0036	0.9918	3.5
18.02.2025	0.028	-0.001	0.9998	3.5
27.05.2025	0.0269	0.0119	0.99	6.5
04.06.2025	0.0218	0.0009	0.99	6.5

Table A2: Total ws-Fe concentration depending on extraction time in acidified water (pH 4.5)

	1 min	5 min	10 min	30 min
Filter B5 22.-23.03.2025: Total ws-Fe [ng m^{-3}]	2.1	4.1	6.0	22.7
Filter B6 23.-24.03.2025: Total ws-Fe [ng m^{-3}]	4.01	6.9	11.5	18.5
Filter B7 24.-25.03.2025: Total ws-Fe [ng m^{-3}]	14.1	17.5	26.7	24.6
Filter B8 25.-26.03.2025: Total ws-Fe [ng m^{-3}]	5.7	7.0	13.9	18.2

https://doi.org/10.5194/ar-2025-37
Preprint. Discussion started: 12 November 2025

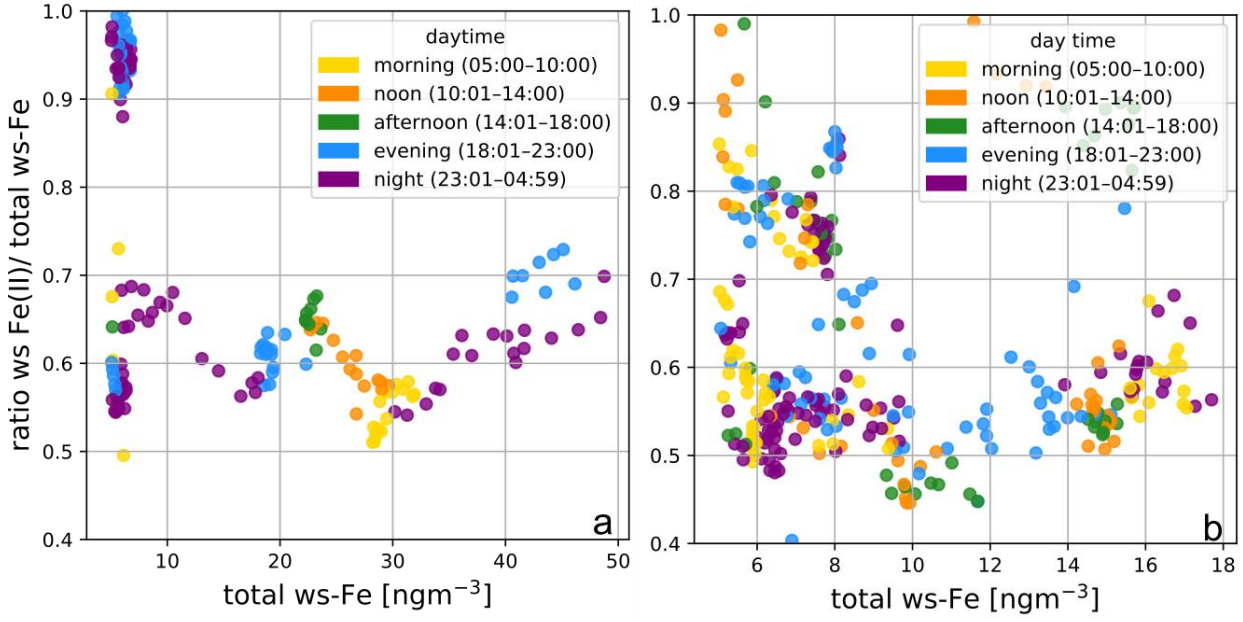

Figure A1: Ratios of ws-Fe(II) to total ws-Fe over total ws-Fe concentration > 5ngm^{-3} coloured depending on time of the day at a) Straße des 17. Juni and b) on the campus of TU Berlin

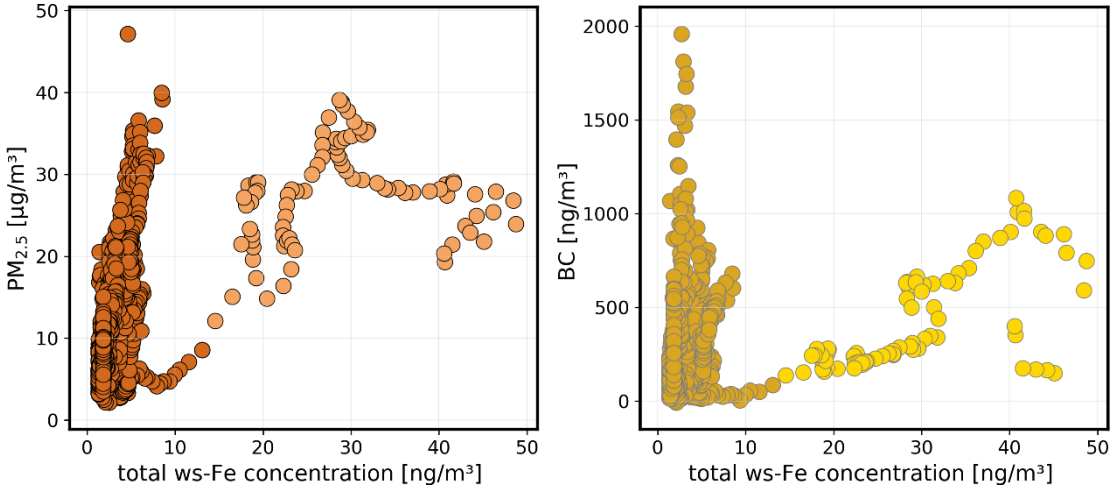

Figure A2: Total ws-Fe concentration to PM2.5 concentrations (left) and BC concentrations (right)

https://doi.org/10.5194/ar-2025-37
Preprint. Discussion started: 12 November 2025

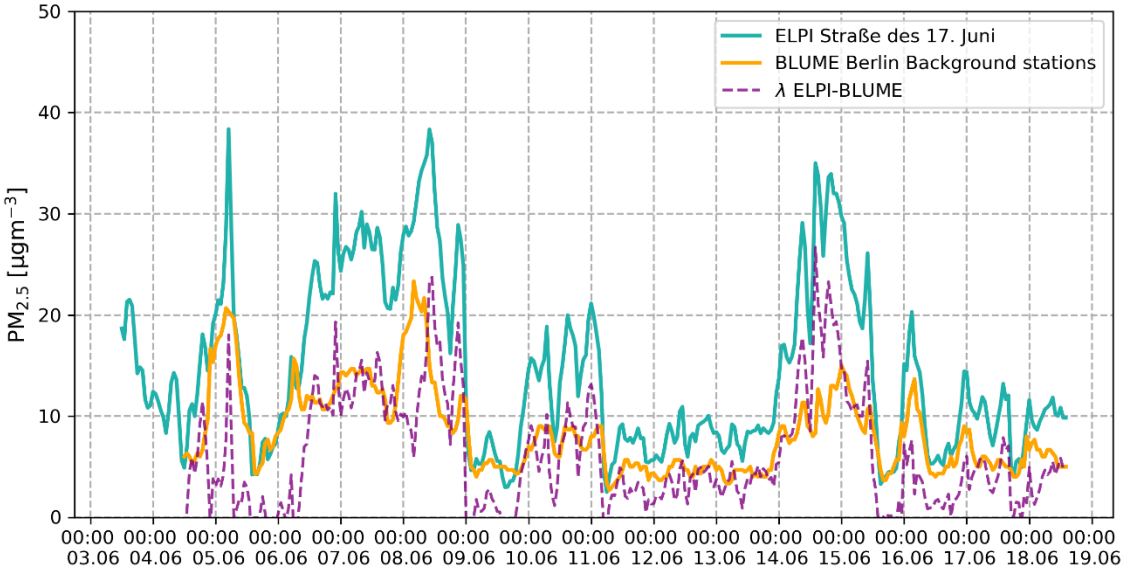

Figure A3: Temporal variability of $PM_{2.5}$ concentrations at Straße des 17. Juni (turquoise) and average concentrations from background stations Neukölln, Mitte and Wedding from Berlin BLUME air quality network (yellow). The purple dashed lines represent the difference between the ELPI measurements at Straße des 17. Juni and the averaged concentrations from BLUME air quality network.

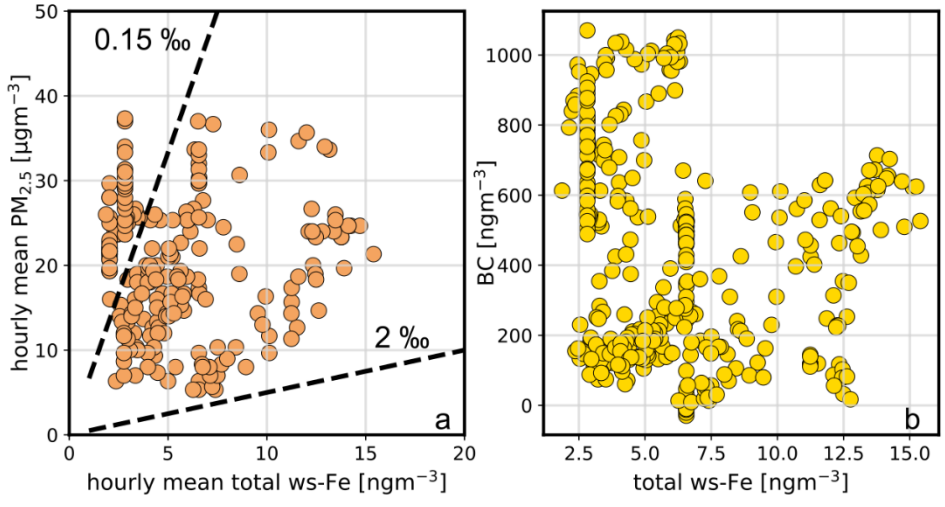

Figure A4: Hourly averaged $PM_{2.5}$ concentration from BLUME background stations over hourly averaged total ws-Fe concentration (a) and BC concentration over total ws-Fe concentrations (b).

https://doi.org/10.5194/ar-2025-37
Preprint. Discussion started: 12 November 2025

References

Al-Abadleh, H. A.: Iron content in aerosol particles and its impact on atmospheric chemistry, Chem. Commun., 60, 1840–1855, https://doi.org/10.1039/D3CC04614A, 2024.

Al-Abadleh, H. A., Smith, M., Ogilvie, A., and Sadiq, N. W.: Quantifying the Effect of Basic Minerals on Acid- and Ligand-Promoted Dissolution Kinetics of Iron in Simulated Dark Atmospheric Aging of Dust and Coal Fly Ash Particles, J. Phys. Chem. A, 128, 8198–8208, https://doi.org/10.1021/acs.jpca.4c05181, 2024.

Arakaki, T. and Faust, B. C.: Sources, sinks, and mechanisms of hydroxyl radical (•OH) photoproduction and consumption in authentic acidic continental cloud waters from Whiteface Mountain, New York: The role of the Fe(r) (r = II, III) photochemical cycle, Journal of Geophysical Research: Atmospheres, 103, 3487–3504, https://doi.org/10.1029/97JD02795, 1998.

Baldo, C., Ito, A., Krom, M. D., Li, W., Jones, T., Drake, N., Ignatyev, K., Davidson, N., and Shi, Z.: Iron from coal combustion particles dissolves much faster than mineral dust under simulated atmospheric acidic conditions, Atmospheric Chemistry and Physics, 22, 6045–6066, https://doi.org/10.5194/acp-22-6045-2022, 2022.

Balsamo Crespo, E., Reichelt-Brushett, A., Smith, R. E. W., Rose, A. L., and Batley, G. E.: Improving the Measurement of Iron(III) Bioavailability in Freshwater Samples: Methods and Performance, Environ Toxicol Chem, 42, 303–316, https://doi.org/10.1002/etc.5530, 2023.

Bianco, A., Passananti, M., Brigante, M., and Mailhot, G.: Photochemistry of the Cloud Aqueous Phase: A Review, Molecules, 25, 423, https://doi.org/10.3390/molecules25020423, 2020.

Browning, T. J. and Moore, C. M.: Global analysis of ocean phytoplankton nutrient limitation reveals high prevalence of co-limitation, Nat Commun, 14, 5014, https://doi.org/10.1038/s41467-023-40774-0, 2023.

Chen, H. and Grassian, V. H.: Iron Dissolution of Dust Source Materials during Simulated Acidic Processing: The Effect of Sulfuric, Acetic, and Oxalic Acids, Environ. Sci. Technol., 47, 10312–10321, https://doi.org/10.1021/es401285s, 2013.

Chen, Y. and Siefert, R. L.: Determination of various types of labile atmospheric iron over remote oceans, Journal of Geophysical Research: Atmospheres, 108, https://doi.org/10.1029/2003JD003515, 2003.

Chu, B., Liggio, J., Liu, Y., He, H., Takekawa, H., Li, S.-M., and Hao, J.: Influence of metal-mediated aerosol-phase oxidation on secondary organic aerosol formation from the ozonolysis and OH-oxidation of α-pinene, Sci Rep, 7, 40311, https://doi.org/10.1038/srep40311, 2017.

Crazzolara, C. and Held, A.: Development of a cascade impactor optimized for size-fractionated analysis of aerosol metal content by total reflection X-ray fluorescence spectroscopy (TXRF), Atmospheric Measurement Techniques, 17, 2183–2194, https://doi.org/10.5194/amt-17-2183-2024, 2024.

De Haan, D. O., Hawkins, L. N., Weber, J. A., Moul, B. T., Hui, S., Cox, S. A., Esse, J. U., Skochdopole, N. R., Lynch, C. P., De Haan, A. C., Le, C., Cazaunau, M., Bergé, A., Pangui, E., Heuser, J., Doussin, J.-F., and Picquet-Varrault, B.: Brown Carbon Aerosol Formation by Multiphase Catechol Photooxidation in the Presence of Soluble Iron, ACS EST Air, 1, 909–917, https://doi.org/10.1021/acsestair.4c00045, 2024.

https://doi.org/10.5194/ar-2025-37
Preprint. Discussion started: 12 November 2025

Deguillaume, L., Leriche, M., Desboeufs, K., Mailhot, G., George, C., and Chaumerliac, N.: Transition Metals in Atmospheric Liquid Phases: Sources, Reactivity, and Sensitive Parameters, Chem. Rev., 105, 3388–3431, https://doi.org/10.1021/cr040649c, 2005.

Fan, S.-M., Moxim, W. J., and Levy II, H.: Aeolian input of bioavailable iron to the ocean, Geophysical Research Letters, 33, https://doi.org/10.1029/2005GL024852, 2006.

Fenton, H. J. J.: Oxidation of tartaric acid in presence... - Google Scholar, Journal of the Chemical Society, Transactions, 899–910, 1894.

Fu, H., Lin, J., Shang, G., Dong, W., Grassian, V. H., Carmichael, G. R., Li, Y., and Chen, J.: Solubility of Iron from Combustion Source Particles in Acidic Media Linked to Iron Speciation, Environ. Sci. Technol., 46, 11119–11127, https://doi.org/10.1021/es302558m, 2012.

Gao, Y., Marsay, C. M., Yu, S., Fan, S., Mukherjee, P., Buck, C. S., and Landing, W. M.: Particle-Size Variability of Aerosol Iron and Impact on Iron Solubility and Dry Deposition Fluxes to the Arctic Ocean, Sci Rep, 9, 16653, https://doi.org/10.1038/s41598-019-52468-z, 2019.

Gao, Y., Yu, S., Sherrell, R. M., Fan, S., Bu, K., and Anderson, J. R.: Particle-Size Distributions and Solubility of Aerosol Iron Over the Antarctic Peninsula During Austral Summer, Journal of Geophysical Research: Atmospheres, 125, e2019JD032082, https://doi.org/10.1029/2019JD032082, 2020.

Giorio, C., Borca, C. N., Zherebker, A., D'Aronco, S., Saidikova, M., Sheikh, H. A., Harrison, R. J., Badocco, D., Soldà, L., Pastore, P., Ammann, M., and Huthwelker, T.: Iron Speciation in Urban Atmospheric Aerosols: Comparison between Thermodynamic Modeling and Direct Measurements, ACS Earth Space Chem., 9, 649–661, https://doi.org/10.1021/acsearthspacechem.4c00359, 2025.

Herrmann, H., Schaefer, T., Tilgner, A., Styler, S. A., Weller, C., Teich, M., and Otto, T.: Tropospheric Aqueous-Phase Chemistry: Kinetics, Mechanisms, and Its Coupling to a Changing Gas Phase, Chem. Rev., 115, 4259–4334, https://doi.org/10.1021/cr500447k, 2015.

Hutchins, D. A. and Tagliabue, A.: Feedbacks between phytoplankton and nutrient cycles in a warming ocean, Nat. Geosci., 17, 495–502, https://doi.org/10.1038/s41561-024-01454-w, 2024.

Ito, A.: Atmospheric Processing of Combustion Aerosols as a Source of Bioavailable Iron, Environ. Sci. Technol. Lett., 2, 70–75, https://doi.org/10.1021/acs.estlett.5b00007, 2015.

Ito, A. and Shi, Z.: Delivery of anthropogenic bioavailable iron from mineral dust and combustion aerosols to the ocean, Atmospheric Chemistry and Physics, 16, 85–99, https://doi.org/10.5194/acp-16-85-2016, 2016.

Ito, A., Myriokefalitakis, S., Kanakidou, M., Mahowald, N. M., Scanza, R. A., Hamilton, D. S., Baker, A. R., Jickells, T., Sarin, M., Bikkina, S., Gao, Y., Shelley, R. U., Buck, C. S., Landing, W. M., Bowie, A. R., Perron, M. M. G., Guieu, C., Meskhidze, N., Johnson, M. S., Feng, Y., Kok, J. F., Nenes, A., and Duce, R. A.: Pyrogenic iron: The missing link to high iron solubility in aerosols, Science Advances, 5, eaau7671, https://doi.org/10.1126/sciadv.aau7671, 2019.

Jickells, T. D., An, Z. S., Andersen, K. K., Baker, A. R., Bergametti, G., Brooks, N., Cao, J. J., Boyd, P. W., Duce, R. A., Hunter, K. A., Kawahata, H., Kubilay, N., laRoche, J., Liss, P. S., Mahowald, N., Prospero, J. M., Ridgwell, A. J., Tegen, I., and Torres, R.: Global Iron Connections Between Desert Dust, Ocean Biogeochemistry, and Climate, Science, 308, 67–71, https://doi.org/10.1126/science.1105959, 2005.

https://doi.org/10.5194/ar-2025-37
Preprint. Discussion started: 12 November 2025

Journet, E., Desboeufs, K. V., Caquineau, S., and Colin, J.-L.: Mineralogy as a critical factor of dust iron solubility, Geophysical Research Letters, 35, https://doi.org/10.1029/2007GL031589, 2008.

Kuang, X. M., Scott ,John A., da Rocha ,Gisele O., Betha ,Raghu, Price ,Derek J., Russell ,Lynn M., Cocker ,David R., and and Paulson, S. E.: Hydroxyl radical formation and soluble trace metal content in particulate matter from renewable diesel and ultra low sulfur diesel in at-sea operations of a research vessel, Aerosol Science and Technology, 51, 147–158, https://doi.org/10.1080/02786826.2016.1271938, 2017.

Kuang, X. M., Gonzalez, D. H., Scott, J. A., Vu, K., Hasson, A., Charbouillot, T., Hawkins, L., and Paulson, S. E.: Cloud Water Chemistry Associated with Urban Aerosols: Rapid Hydroxyl Radical Formation, Soluble Metals, Fe(II), Fe(III), and Quinones, ACS Earth Space Chem., 4, 67–76, https://doi.org/10.1021/acsearthspacechem.9b00243, 2020.

Langmuir, D.: Aqueous environmental geochemistry, New Jersey, 1997.

Lei, Y., Li, D., Lu, D., Zhang, T., Sun, J., Wang, X., Xu, H., and Shen, Z.: Insights into the roles of aerosol soluble iron in secondary aerosol formation, Atmospheric Environment, 294, 119507, https://doi.org/10.1016/j.atmosenv.2022.119507, 2023.

Liu, L., Li, W., Lin, Q., Wang, Y., Zhang, J., Zhu, Y., Yuan, Q., Zhou, S., Zhang, D., Baldo, C., and Shi, Z.: Size-dependent aerosol iron solubility in an urban atmosphere, npj Clim Atmos Sci, 5, 53, https://doi.org/10.1038/s41612-022-00277-z, 2022.

Liu, X. and Millero, F. J.: The solubility of iron hydroxide in sodium chloride solutions, Geochimica et Cosmochimica Acta, 63, 3487–3497, https://doi.org/10.1016/S0016-7037(99)00270-7, 1999.

Liu, X. and Millero, F. J.: The solubility of iron in seawater, Marine Chemistry, 77, 43–54, https://doi.org/10.1016/S0304-4203(01)00074-3, 2002.

Longo, A. F., Feng, Y., Lai, B., Landing, W. M., Shelley, R. U., Nenes, A., Mihalopoulos, N., Violaki, K., and Ingall, E. D.: Influence of Atmospheric Processes on the Solubility and Composition of Iron in Saharan Dust, Environ. Sci. Technol., 50, 6912–6920, https://doi.org/10.1021/acs.est.6b02605, 2016.

Lüchtrath, S., Klemer, S., Dubois, C., George, C., and Held, A.: Impact of atmospheric water-soluble iron on α-pinene-derived SOA formation and transformation in the presence of aqueous droplets, Environmental Science: Atmospheres, 4, 1218–1228, https://doi.org/10.1039/D4EA00095A, 2024.

Lüchtrath, S., Wutke, R., and Held, A.: Secondary Formation of Light-Absorbing, Insoluble Particles from Catechol in the Presence of Fe(II) or Fe(III) and Hydrogen Peroxide at Dark and Light Conditions, ACS EST Air, https://doi.org/10.1021/acsestair.5c00091, 2025.

Luo, C., Mahowald, N. M., Meskhidze, N., Chen, Y., Siefert, R. L., Baker, A. R., and Johansen, A. M.: Estimation of iron solubility from observations and a global aerosol model, J. Geophys. Res., 110, 2005JD006059, https://doi.org/10.1029/2005JD006059, 2005.

Luo, C., Mahowald, N., Bond, T., Chuang, P. Y., Artaxo, P., Siefert, R., Chen, Y., and Schauer, J.: Combustion iron distribution and deposition, Global Biogeochemical Cycles, 22, https://doi.org/10.1029/2007GB002964, 2008.

Ma, Y.: Developments and improvements to the particle-into-liquid sampler (PILS) and its application to Asian outflow studies, Georgia Institute of Technology, 2004.

Mahowald, N. M., Engelstaedter, S., Luo, C., Sealy, A., Artaxo, P., Benitez-Nelson, C., Bonnet, S., Chen, Y., Chuang, P. Y., Cohen, D. D., Dulac, F., Herut, B., Johansen, A. M., Kubilay, N., Losno, R., Maenhaut, W., Paytan, A., Prospero, J. M., Shank,

https://doi.org/10.5194/ar-2025-37
Preprint. Discussion started: 12 November 2025

L. M., and Siefert, R. L.: Atmospheric Iron Deposition: Global Distribution, Variability, and Human Perturbations*, Annual Review of Marine Science, 1, 245–278, https://doi.org/10.1146/annurev.marine.010908.163727, 2009.

Majestic, B. J., Schauer, J. J., Shafer, M. M., Turner, J. R., Fine, P. M., Singh, M., and Sioutas, C.: Development of a Wet-Chemical Method for the Speciation of Iron in Atmospheric Aerosols, Environ. Sci. Technol., 40, 2346–2351, https://doi.org/10.1021/es052023p, 2006.

Meskhidze, N., Hurley, D., Royalty, T. M., and Johnson, M. S.: Potential effect of atmospheric dissolved organic carbon on the iron solubility in seawater, Marine Chemistry, 194, 124–132, https://doi.org/10.1016/j.marchem.2017.05.011, 2017.

Millero, F. J., Sotolongo, S., and Izaguirre, M.: The oxidation kinetics of Fe(II) in seawater, Geochimica et Cosmochimica Acta, 51, 793–801, https://doi.org/10.1016/0016-7037(87)90093-7, 1987.

Moore, C. M., Mills, M. M., Arrigo, K. R., Berman-Frank, I., Bopp, L., Boyd, P. W., Galbraith, E. D., Geider, R. J., Guieu, C., Jaccard, S. L., Jickells, T. D., La Roche, J., Lenton, T. M., Mahowald, N. M., Marañón, E., Marinov, I., Moore, J. K., Nakatsuka, T., Oschlies, A., Saito, M. A., Thingstad, T. F., Tsuda, A., and Ulloa, O.: Processes and patterns of oceanic nutrient limitation, Nature Geosci, 6, 701–710, https://doi.org/10.1038/ngeo1765, 2013.

Murray, J. W. and Gill, G.: The geochemistry of iron in puget sound, Geochimica et Cosmochimica Acta, 42, 9–19, https://doi.org/10.1016/0016-7037(78)90211-9, 1978.

Nagy, G., Fehér, Zs., and Pungor, E.: Application of silicone rubber-based graphite electrodes for continuous flow measurements: Part II. Voltammetric study of active substances injected into electrolyte streams, Analytica Chimica Acta, 52, 47–54, https://doi.org/10.1016/S0003-2670(01)80040-4, 1970.

Oakes, M., Rastogi, N., Majestic, B. J., Shafer, M., Schauer, J. J., Edgerton, E. S., and Weber, R. J.: Characterization of soluble iron in urban aerosols using near-real time data, Journal of Geophysical Research: Atmospheres, 115, https://doi.org/10.1029/2009JD012532, 2010.

O'Connor, T. C., Jennings, S. G., and O'Dowd, C. D.: Highlights of fifty years of atmospheric aerosol research at Mace Head, Atmospheric Research, 90, 338–355, https://doi.org/10.1016/j.atmosres.2008.08.014, 2008.

Orsini, D. A., Ma, Y., Sullivan, A., Sierau, B., Baumann, K., and Weber, R. J.: Refinements to the particle-into-liquid sampler (PILS) for ground and airborne measurements of water soluble aerosol composition, Atmospheric Environment, 37, 1243–1259, https://doi.org/10.1016/S1352-2310(02)01015-4, 2003.

Paris, R. and Desboeufs, K. V.: Effect of atmospheric organic complexation on iron-bearing dust solubility, Atmospheric Chemistry and Physics, 13, 4895–4905, https://doi.org/10.5194/acp-13-4895-2013, 2013.

Pascual-Reguera, M. I., Ortega-Carmona, I., and Molina-Díaz, A.: Spectrophotometric determination of iron with ferrozine by flow-injection analysis, Talanta, 44, 1793–1801, https://doi.org/10.1016/S0039-9140(97)00050-7, 1997.

Pehkonen, S. O., Siefert, R., Erel, Y., Webb, S., and Hoffmann, M. R.: Photoreduction of iron oxyhydroxides in the presence of important atmospheric organic compounds, Environ. Sci. Technol., 27, 2056–2062, https://doi.org/10.1021/es00047a010, 1993.

Pham, A. N. and Waite, T. D.: Oxygenation of Fe(II) in natural waters revisited: Kinetic modeling approaches, rate constant estimation and the importance of various reaction pathways, Geochimica et Cosmochimica Acta, 72, 3616–3630, https://doi.org/10.1016/j.gca.2008.05.032, 2008.

https://doi.org/10.5194/ar-2025-37
Preprint. Discussion started: 12 November 2025

Pullin, M. J. and Cabaniss, S. E.: Colorimetric flow-injection analysis of dissolved iron in high DOC waters, Water Research, 35, 363–372, https://doi.org/10.1016/S0043-1354(00)00259-1, 2001.

Pye, H. O. T., Nenes, A., Alexander, B., Ault, A. P., Barth, M. C., Clegg, S. L., Collett Jr., J. L., Fahey, K. M., Hennigan, C. J., Herrmann, H., Kanakidou, M., Kelly, J. T., Ku, I.-T., McNeill, V. F., Riemer, N., Schaefer, T., Shi, G., Tilgner, A., Walker, J. T., Wang, T., Weber, R., Xing, J., Zaveri, R. A., and Zuend, A.: The acidity of atmospheric particles and clouds, Atmospheric Chemistry and Physics, 20, 4809–4888, https://doi.org/10.5194/acp-20-4809-2020, 2020.

Raiswell, R., Benning, L. G., Tranter, M., and Tulaczyk, S.: Bioavailable iron in the Southern Ocean: the significance of the iceberg conveyor belt, Geochem Trans, 9, 7, https://doi.org/10.1186/1467-4866-9-7, 2008.

Rastogi, N., Oakes, M. M., Schauer, J. J., Shafer, M. M., Majestic, B. J., and Weber, R. J.: New Technique for Online Measurement of Water-Soluble Fe(II) in Atmospheric Aerosols, Environ. Sci. Technol., 43, 2425–2430, https://doi.org/10.1021/es8031902, 2009.

Rubasinghege, G., Lentz, R. W., Scherer, M. M., and Grassian, V. H.: Simulated atmospheric processing of iron oxyhydroxide minerals at low pH: Roles of particle size and acid anion in iron dissolution, Proceedings of the National Academy of Sciences, 107, 6628–6633, https://doi.org/10.1073/pnas.0910809107, 2010.

Salazar, J. R., Pfotenhauer, D. J., Leresche, F., Rosario-Ortiz, F. L., Hannigan, M. P., Fakra, S. C., and Majestic, B. J.: Iron Speciation in PM2.5 From Urban, Agriculture, and Mixed Environments in Colorado, USA, Earth and Space Science, 7, e2020EA001262, https://doi.org/10.1029/2020EA001262, 2020a.

Salazar, J. R., Cartledge, B. T., Haynes, J. P., York-Marini, R., Robinson, A. L., Drozd, G. T., Goldstein, A. H., Fakra, S. C., and Majestic, B. J.: Water-soluble iron emitted from vehicle exhaust is linked to primary speciated organic compounds, Atmospheric Chemistry and Physics, 20, 1849–1860, https://doi.org/10.5194/acp-20-1849-2020, 2020b.

Shao, Y., Wyrwoll, K.-H., Chappell, A., Huang, J., Lin, Z., McTainsh, G. H., Mikami, M., Tanaka, T. Y., Wang, X., and Yoon, S.: Dust cycle: An emerging core theme in Earth system science, Aeolian Research, 2, 181–204, https://doi.org/10.1016/j.aeolia.2011.02.001, 2011.

Shi, Z., Krom, M. D., Jickells, T. D., Bonneville, S., Carslaw, K. S., Mihalopoulos, N., Baker, A. R., and Benning, L. G.: Impacts on iron solubility in the mineral dust by processes in the source region and the atmosphere: A review, Aeolian Research, 5, 21–42, https://doi.org/10.1016/j.aeolia.2012.03.001, 2012.

Shi, Z., Krom, M. D., Bonneville, S., and Benning, L. G.: Atmospheric Processing Outside Clouds Increases Soluble Iron in Mineral Dust, Environ. Sci. Technol., 49, 1472–1477, https://doi.org/10.1021/es504623x, 2015.

Sholkovitz, E. R., Sedwick, P. N., and Church, T. M.: Influence of anthropogenic combustion emissions on the deposition of soluble aerosol iron to the ocean: Empirical estimates for island sites in the North Atlantic, Geochimica et Cosmochimica Acta, 73, 3981–4003, https://doi.org/10.1016/j.gca.2009.04.029, 2009.

S. Hopstock, K., P. Carpenter, B., P. Patterson, J., A. Al-Abadleh, H., and A. Nizkorodov, S.: Formation of insoluble brown carbon through iron-catalyzed reaction of biomass burning organics, Environmental Science: Atmospheres, 3, 207–220, https://doi.org/10.1039/D2EA00141A, 2023.

Slikboer, S., Grandy, L., Blair, S. L., Nizkorodov, S. A., Smith, R. W., and Al-Abadleh, H. A.: Formation of Light Absorbing Soluble Secondary Organics and Insoluble Polymeric Particles from the Dark Reaction of Catechol and Guaiacol with Fe(III), Environ. Sci. Technol., 49, 7793–7801, https://doi.org/10.1021/acs.est.5b01032, 2015.

https://doi.org/10.5194/ar-2025-37
Preprint. Discussion started: 12 November 2025

Sorooshian, A., Brechtel, F. J., Ma, Y., Weber, R. J., Corless, A., Flagan, R. C., and Seinfeld, J. H.: Modeling and Characterization of a Particle-into-Liquid Sampler (PILS), Aerosol Science and Technology, 40, 396–409, https://doi.org/10.1080/02786820600632282, 2006.

Stieger, B., Spindler, G., Fahlbusch, B., Müller, K., Grüner, A., Poulain, L., Thöni, L., Seitler, E., Wallasch, M., and Herrmann, H.: Measurements of PM10 ions and trace gases with the online system MARGA at the research station Melpitz in Germany – A five-year study, J Atmos Chem, 75, 33–70, https://doi.org/10.1007/s10874-017-9361-0, 2018.

Stieger, B., Spindler, G., van Pinxteren, D., Grüner, A., Wallasch, M., and Herrmann, H.: Development of an online-coupled MARGA upgrade for the 2 h interval quantification of low-molecular-weight organic acids in the gas and particle phases, Atmospheric Measurement Techniques, 12, 281–298, https://doi.org/10.5194/amt-12-281-2019, 2019.

Stookey, L. L.: Ferrozine---a new spectrophotometric reagent for iron, Anal. Chem., 42, 779–781, https://doi.org/10.1021/ac60289a016, 1970.

Tilgner, A. and Herrmann, H.: Tropospheric Aqueous-Phase OH Oxidation Chemistry: Current Understanding, Uptake of Highly Oxidized Organics and Its Effects, in: Multiphase Environmental Chemistry in the Atmosphere, vol. 1299, American Chemical Society, 49–85, https://doi.org/10.1021/bk-2018-1299.ch004, 2018.

Valavanidis, A., Salika, A., and Theodoropoulou, A.: Generation of hydroxyl radicals by urban suspended particulate air matter. The role of iron ions, Atmospheric Environment, 34, 2379–2386, https://doi.org/10.1016/S1352-2310(99)00435-5, 2000.

Wang, X., Shen, Z., Huang, S., Che, H., Zhang, L., Lei, Y., Sun, J., Shen, G., Xu, H., and Cao, J.: Water-soluble iron in PM2.5 in winter over six Chinese megacities: Distributions, sources, and environmental implications, Environmental Pollution, 314, 120329, https://doi.org/10.1016/j.envpol.2022.120329, 2022.

Weber, R. J., Orsini, D., Daun, Y., Lee, Y.-N., Klotz, P. J., and Brechtel, F.: A Particle-into-Liquid Collector for Rapid Measurement of Aerosol Bulk Chemical Composition, Aerosol Science and Technology, 35, 718–727, https://doi.org/10.1080/02786820152546761, 2001.

Yang, Y., Gao, D., and Weber, R. J.: A Method for Liquid Spectrophotometric Measurement of VariousForms of Iron and Copper in Ambient Aerosols, https://doi.org/10.5194/amt-2021-72, 9 March 2021.

Zeng, L., Sullivan, A. P., Washenfelder, R. A., Dibb, J., Scheuer, E., Campos, T. L., Katich, J. M., Levin, E., Robinson, M. A., and Weber, R. J.: Assessment of online water-soluble brown carbon measuring systems for aircraft sampling, Atmospheric Measurement Techniques, 14, 6357–6378, https://doi.org/10.5194/amt-14-6357-2021, 2021.

Zepp, R. G., Faust, B. C., and Hoigne, J.: Hydroxyl radical formation in aqueous reactions (pH 3-8) of iron(II) with hydrogen peroxide: the photo-Fenton reaction, Environ. Sci. Technol., 26, 313–319, https://doi.org/10.1021/es00026a011, 1992.

Zhang, J.-Z., Kelble, C., and Millero, F. J.: Gas-segmented continuous flow analysis of iron in water with a long liquid waveguide capillary flow cell, Analytica Chimica Acta, 438, 49–57, https://doi.org/10.1016/S0003-2670(01)01031-5, 2001.